mathematics

MDPI

Article

Development of Slime Mold Optimizer with Application for Tuning Cascaded PD-PI Controller to Enhance Frequency Stability in Power Systems

Slim Abid [1,2], Ali M. El-Rifaie [3,*], Mostafa Elshahed [4,5,*], Ahmed R. Ginidi [6], Abdullah M. Shaheen [6], Ghareeb Moustafa [1,7] and Mohamed A. Tolba [8,9]

1 Electrical Engineering Department, Jazan University, Jazan 45142, Saudi Arabia; smabid@jazanu.edu.sa (S.A.); gmoustafa@jazanu.edu.sa (G.M.)
2 Ecole Nationale d'Ingénieurs de Sfax, ENIS, Sfax 3038, Tunisia
3 College of Engineering and Technology, American University of the Middle East, Egaila 54200, Kuwait
4 Electrical Engineering Department, Engineering and Information Technology College, Buraydah Private Colleges, Buraydah 51418, Saudi Arabia
5 Electrical Power Engineering Department, Faculty of Engineering, Cairo University, Giza 12613, Egypt
6 Department of Electrical Power Engineering, Faculty of Engineering, Suez University, Suez 43533, Egypt; ahmed.ginidi@eng.suezuni.edu.eg (A.R.G.); abdullah.mohamed.eng19@suezuni.edu.eg (A.M.S.)
7 Electrical Engineering Department, Suez Canal University, Ismailia 41522, Egypt
8 Reactors Department, Nuclear Research Center, Egyptian Atomic Energy Authority, Cairo 11787, Egypt; matolba@eaea.org.eg
9 Electrical Power Systems Department, National Research University "MPEI", 111250 Moscow, Russia
* Correspondence: ali.el-rifaie@aum.edu.kw (A.M.E.-R.); mostafa.elshahed@bpc.edu.sa (M.E.)

Abstract: Multi-area power systems (MAPSs) are highly complex non-linear systems facing a fundamental issue in real-world engineering problems called frequency stability problems (FSP). This paper develops an enhanced slime mold optimization algorithm (ESMOA) to optimize the tuning parameters for a cascaded proportional derivative-proportional integral (PD-PI) controller. The novel ESMOA proposal includes a new system that combines basic SMO, chaotic dynamics, and an elite group. The motion update incorporates the chaotic technique, and the exploitation procedure is enhanced by searching for a select group rather than merely the best solution overall. The proposed cascaded PD-PI controller based on the ESMOA is employed for solving the FSP in MAPSs with two area non-reheat thermal systems to keep the balance between the electrical power load and the generation and provide power system security, reliability, and quality. The proposed cascaded PD-PI controller based on the ESMOA is evaluated using time domain simulation to minimize the integral time-multiplied absolute error (ITAE). It is evaluated in four different test situations with various sets of perturbations. For tuning the cascaded PD-PI controller, the proposed ESMOA is compared to the golden search optimizer (GSO) and circle optimizer (CO), where the proposed ESMOA provides the best performance. Furthermore, the findings of the proposed cascaded PD-PI controller based on the ESMOA outperform previous published PID and PI controllers adjusted using numerous contemporary techniques.

Keywords: load frequency control; cascaded proportional derivative-proportional integral (PD-PI) controller; slime mold optimization algorithm; PID controller

MSC: 93C10

Citation: Abid, S.; El-Rifaie, A.M.; Elshahed, M.; Ginidi, A.R.; Shaheen, A.M.; Moustafa, G.; Tolba, M.A. Development of Slime Mold Optimizer with Application for Tuning Cascaded PD-PI Controller to Enhance Frequency Stability in Power Systems. *Mathematics* **2023**, *11*, 1796. https://doi.org/10.3390/math11081796

Academic Editors: Fang Liu and Qianyi Liu

Received: 28 February 2023
Revised: 2 April 2023
Accepted: 7 April 2023
Published: 10 April 2023

1. Introduction

A continuous production of electrical energy, supplied by power-generating plants, has grown into a requirement for modernized life and the industrial progress of countries. A stable power network can endure interruptions, fluctuations, and changing consumer needs.

If the electrical network becomes unstable, load shedding might be activated, leading to blackouts in the worst-case scenario. Loads in electrical networks are particularly uncertain and variable due to changes in load demand, which causes the network frequency and tie-line transfer power to deviate from the nominal levels [1,2]. Power networks are typically integrated with several power-generating areas to deliver electricity to high-demand zones. A disruption in one location may impact the other related power systems [3]. The primary purpose of multi-area power systems (MAPSs) aims at balancing supply and connected loads, which is an important challenge to managing the continual growth in demand and the peculiarities of the MAPSs system, which incorporates a diversity of power station types [4]. As a result, a power network operator's primary priority is maintaining the frequency of a power system. Area generation control (AGC) can be designed to restore the system to its steady state by regulating the generator output power and preserving a balance between power production and load requirements [5,6]. This problem becomes more and more critical with the integration of renewable sources [7], flexible alternating current devices [8], high voltage direct current grids [9], batteries [10], automatic voltage regulators [11], etc.

In MAPSs, frequency stability or load frequency control (LFC) is the process that keeps the frequency inside nominal boundaries when the load demand changes. LFC is critical to power system stability because it preserves power balancing across linked regions despite varying loading situations. When the system's loading surpasses or drops short of the generator's power, the system's frequency will become unbalanced and surpass the threshold limitations. An automatic control action is performed to preserve the nominal frequency by initiating load shedding or activating protection relays that disconnect generators from the network [12,13]. The frequency of undershoots, overshoots, and settling time must be maintained at a minimum to guarantee dependable power system operation, which may be accomplished by installing external controllers [14].

Over many years, there have been substantial efforts to run numerous optimization techniques to improve the controllers' configurations, while metaheuristic approaches may manage technological obstacles, including complexity, non-linearities, and uncertainties. As a result, the genetic algorithm (GA) was utilized to improve the settings of AGC in a two-area power network having non-reheat thermal generating plants [15]. Although the GA seems relatively robust owing to a more significant standard error of the derived fitness scores, it has been integrated with the Taguchi approach to design the employed AGC via optimally estimating the corresponding gains [15]. In [16], a particle swarm optimization (PSO) containing a constricting component and a craziness-based PSO were utilized to improve the undershoot, overshoot, and settling time of transient response. Furthermore, the differential evolution (DE) approach was employed to update the PI controller in a connected power system to overcome the frequency stability issue [17]. In [18], a flower pollination optimization algorithm (FPOA) was performed in MAPSs to design a proportional-integral-derivative (PID) controller that makes use of spontaneous flower pollinating types. A bacterial foraging method was integrated PSO-dependent on the PI controller for handling the LFC of interconnected MAPSs under standard and customized fitness functions, including two regions of non-reheat thermal systems [19]. In [20], an adaptive sliding mode control mechanism was developed and used for the LFC to withstand unmodeled dynamics, parametric fluctuation, and external disturbances. It also reduces chattering and is used in the LFC regulation based on the power system's diverse areas. Ref. [21] describes grey wolf optimizing implementations for AGC in three MAPSs with and without solar thermal power plants. Furthermore, in [22], the cuckoo search approach was used to solve the LFC problem in three-area connected systems by optimizing the PI controller and the integral plus the double derivative controller based on two degrees of freedom [23].

In [24], a self-adapted multi-population elitist (SAMPE) JAYA compared the optimizing method that was developed for PID controller design as an upgraded JAYA variant to control the LFC in connected two non-reheat thermal MAPSs optimally. In a two-area

connected MAPS, a PID controller based on the optimization approach was used to minimize a single-objective target, including numerous ITAE performance indicators [25]. A teaching learning-based optimizing technique was utilized to adequately design a fuzzy PID controller to manage the undershoot, overshoot, and settling time [26]. Ref. [27] combines an advanced type II fuzzified PID controller with a water cycle algorithm (WCA) and applies it to a MAPS with generation rate limits. To tackle LFC regulation in MAPSs, Ref. [28] created a cascaded PI-PI and PD with filter-PI utilizing the coyote optimization technique. In [29], the bees optimization approach (BOA) was used to optimize the settings of a fuzzed PID comprising a derivative filter, which was then applied to a dual area-linked power system. In [30], a gravitational search method was combined with the firefly optimizing technique to enhance controller setting adjustment and was used in a two-area hydrothermal power system. In [31], the arithmetic optimization approach (AOA) was used to fine-tune a fuzzy-PID controller while accounting for the influence of the high voltage direct current link to overcome the drawbacks of AC transmission.

The slime mold optimization algorithm (SMOA) is an evolutionary approach generated by the propagating and foraging behavior of slime mold, which was reported in 2020 by Li et al. [27]. The SMOA features a distinctive conceptual model, highly efficient outcomes, a gradient-free and simple coding structure that mimics the positive and negative feedbacks of slime mold propagating waves. It is effectively employed for a variety of practical and industrial optimization problems, including engineering design problems [31], load estimation of water resources [30], parameter estimations of fuel cells [29], parameter identification of photovoltaic modules [32,33], optimal power flow [34,35], and emission economic dispatch [36]. The SMOA still has some drawbacks, including low computing accuracy and a premature convergence speed on selected benchmark problems [30]. As a result, in this research, an ESMOA is presented for addressing engineering issues using chaotic dynamics and an elite group. The suggested ESMOA makes two changes to the conventional SMOA to improve its performance. Initially, an elite group is established to save the best solutions for every repetition to improve the exploitative-seeking tactic. Secondly, to improve the exploratory seeking tactic, a logistic mapping with a chaotic tendency is devised to improve the search in extremely random environments. To address the FSP of MAPSs, a cascaded PD-PI controller is optimized utilizing an upgraded ESMOA with two area non-reheat thermal systems. It is evaluated to minimize the ITAE using time domain simulation. The proposed cascaded PD-PI controller based on the ESMOA is evaluated in four test situations with various sets of perturbations. The proposed ESMOA is compared to the golden search optimizer (GSO) [37] and circle optimizer (CO) [38] for adjusting the cascaded PD-PI controller, with the suggested ESMOA providing the best performance. Furthermore, the suggested cascaded PD-PI controller based on the ESMOA outperforms previously reported PID and PI controllers modified with various modern approaches. The following are the primary contributions proposed in this paper:

- The frequency stability of MAPSs is addressed via an innovative cascaded PD-PI controller via ESMOA.
- With SMOA, an elite group and chaotic logistic mapping emerge to produce a novel ESMOA with better performance than recent GSO and CO algorithms.
- The ESMOA has more reliability than contemporary GSO and CO algorithms in designing the cascaded PD-PI controller.
- The proposed PD-PI controller based on the ESMOA outperforms previously reported PID and PI controllers using modern methods.

The following is the structure of the presented article. Section 2 describes the proposed cascaded PD-PI controller and the FSP of MAPSs. Section 3 offers the proposed ESMOA and its stages. Section 4 includes the results and discussion, and Section 5 shows the conclusions.

2. Problem Formulation

MAPS Model

In this study, the MAPS includes two non-reheat thermal turbine generators and employs the proposed cascaded PD-PI controller based on the ESMOA in each area, as depicted in Figure 1. As shown, for each area, the key components are the speed-regulating device, turbine, and generator, as mentioned in Refs. [39,40]. The change in the power demands (ΔP_{D1} and ΔP_{D2}), the change in the tie-line power transfer (ΔP_{TIE}), and the governor controller signals (u_1 and u_2) handle the inputs. At the same time, the frequency deviations in each area (Δf_1 and Δf_2) and the control errors (ACE_1 and ACE_2) represent the outputs [25]. ΔP_g is the change (per unit (p.u)) in the governor valve position; ΔP_t represents the power changes (p.u) in turbine output; T_{12} refers to the synchronized coefficient between the two areas; Δf indicates the frequency change (Hz) in the power system; B indicates the frequency bias; and R refers to the governor speed droop characteristics. In Figure 1, T_{g1}, T_{g2}, T_{t1}, T_{t2}, T_{P1}, and T_{P2} indicate the time constants (in a sec) of the governor, the turbine, and the power system, respectively, of both areas. KP_1 and KP_2 are the power system gains of the two areas, respectively. R_1 and R_2 represent the governor speed regulation constants.

The input signals to the controllers are the respective area control errors (ACE_1 and ACE_2) from

$$ACE_1 = \Delta P_{TIE} + B_1 \times \Delta f_1 \tag{1}$$

$$ACE_2 = a_{12} \times \Delta P_{TIE} + B_2 \times \Delta f_2 \tag{2}$$

With two control loops, the cascaded controller prevents perturbation from expanding to adjacent system parts [41]. As illustrated in Figure 2, the cascaded controller has two control loops (master and slave). The master one represents the outer loop. It contains the process output $y(s)$ that will be influenced by the master control. The load disturbance $\Delta P_D(s)$ influences the power system $G_{PS}(s)$ gain, indicating the outer process.

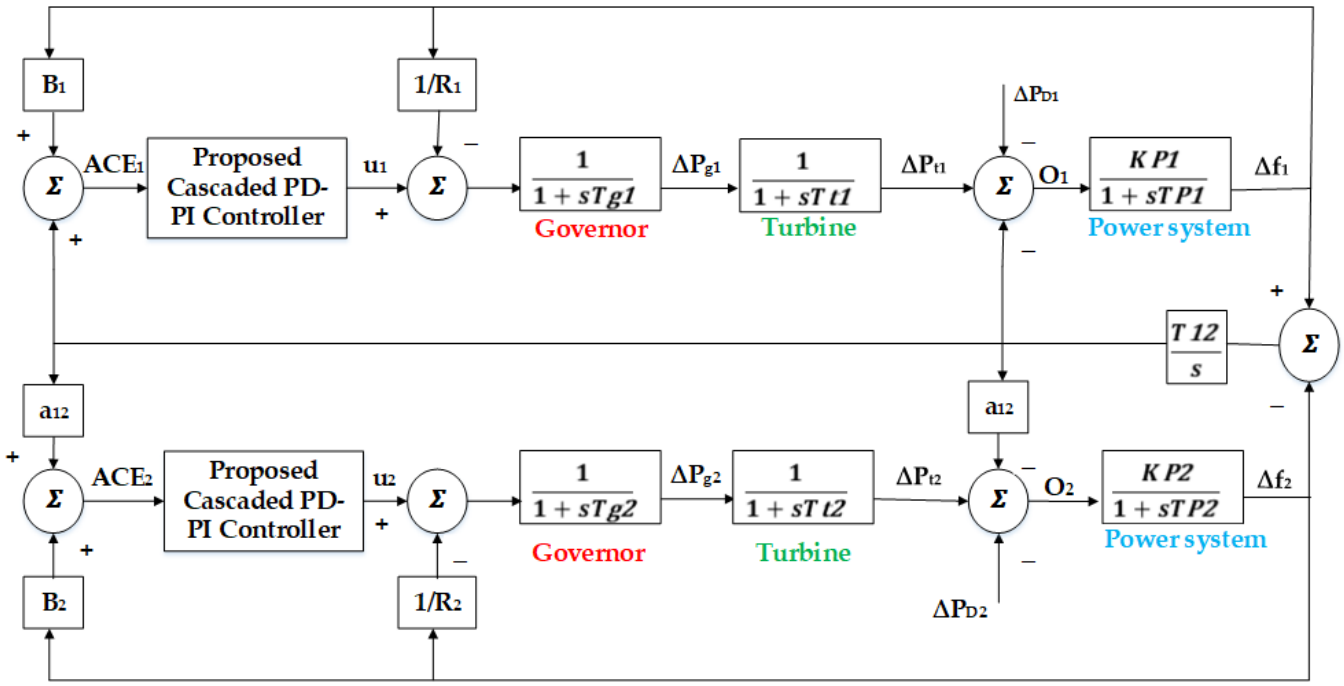

Figure 1. Block diagram for a two-area power system model [25,42].

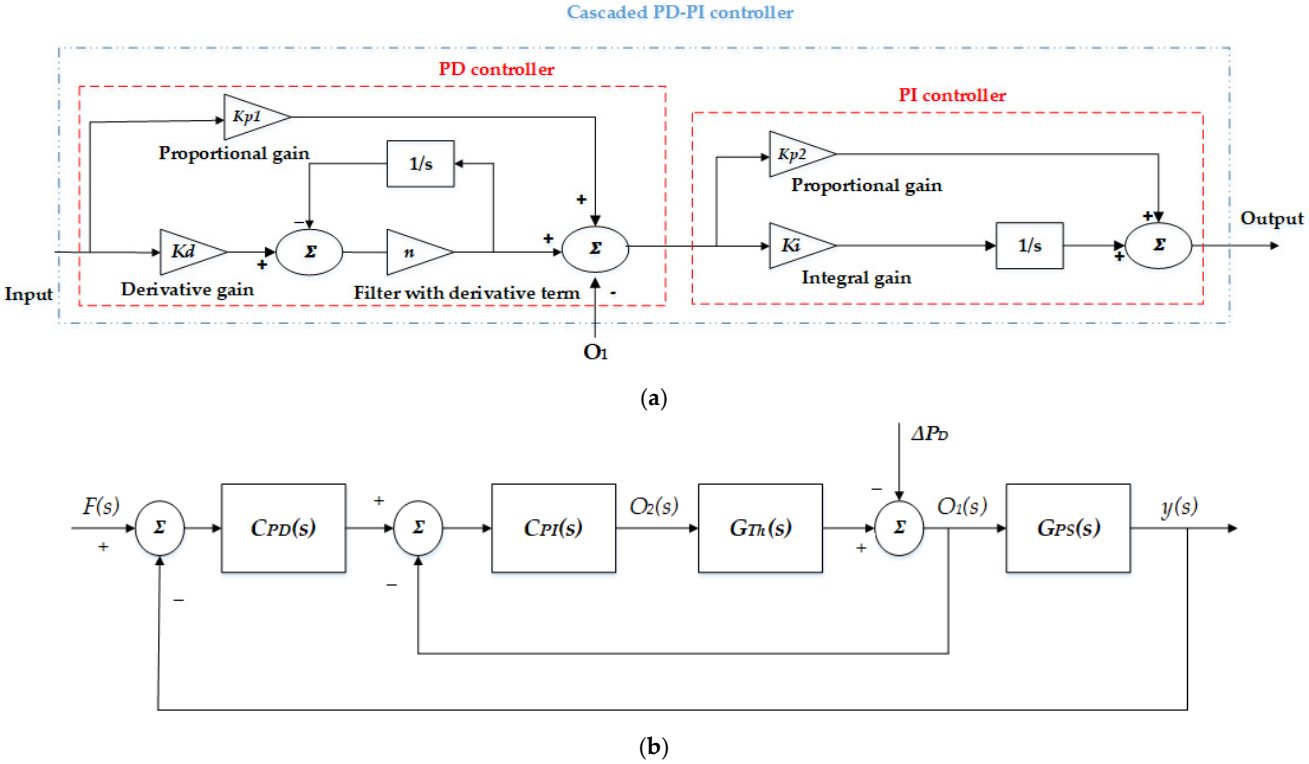

Figure 2. Proposed cascaded PD-PI controller. (**a**) Detailed cascaded PD-PI controller. (**b**) Cascaded PD-PI controller integration with the non-reheat thermal turbine generators and power system.

The master loop formula is as follows:

$$y(s) = G_{PS}(s) \times O_1(s) + \Delta P_D(s) \tag{3}$$

where $O_1(s)$ is the incoming signal to $G_{PS}(s)$, which is also $y_2(s)$ as the process output of the slave loop. $C_{PD}(s)$ is the outer loop controller responsible for $y(s)$ in order to obtain $F(s)$ which is the reference signal. The slave, or inner loop, represents the internal process gain $G_{TH}(s)$. It can be mathematically defined as follows:

$$y_2(s) = G_{TH}(s) \times O_2(s) \tag{4}$$

where $O_2(s)$ denotes the internal process's input signal. The inner loop controller is known as $C_{PI}(s)$. That loop considers the impact of the internal process's gain adjustments.

The cascade controller's whole transfer function may be represented as follows:

$$y(s) = TF1(s) \times F(s) - TF2(s) \times \Delta P_D(s) \tag{5}$$

$$TF1(s) = \left(\frac{G_{PS}(s)G_{TH}(s)C_{PD}(s)C_{PI}(s)}{1 + G_{TH}(s)C_{PI}(s) + G_{PS}(s)G_{TH}(s)C_{PD}(s)C_{PI}(s)} \right) \tag{6}$$

$$TF2(s) = \left(\frac{G_{PS}(s)}{1 + G_{TH}(s)C_{PI}(s) + G_{PS}(s)G_{TH}(s)C_{PD}(s)C_{PI}(s)} \right) \tag{7}$$

As a result, the goal function (OF) is used to disclose the system's needs and constraints to build the proposed cascaded PD-PI controller as effectively as is feasible. Under normal conditions, each area would follow its load, and in the event of a load interruption, the

power exchange between areas would be swiftly recovered to its intended value. A time-domain objective function is adjusted utilizing integral criteria as follows:

$$OF = ITAE = \int_0^{t_{sim}} (|\Delta f_1| + |\Delta f_2| + |\Delta P_{TIE}|) \times t \times dt \tag{8}$$

Furthermore, *OF* can be readily upgraded to minimize the peak overshoots of frequency fluctuations across each area and in tie-line power transmission. This adaptation evolves due to attaining a suitable damping ratio to offer a specific degree of stability [43]. The problem constraints are the boundaries of the controller component settings. Thus, the design task could be represented as the following optimization aspect.

$$Min\ OF \tag{9}$$

Subject to
For the proposed cascaded PD-PI controller,

$$Kp1_{Area,Min} \leq Kp1_{Area} \leq Kp1_{Area,Max},\ Area = 1\ or\ 2 \tag{10}$$

$$Kd_{Area,Min} \leq Kd_{Area} \leq Kd_{Area,Max},\ Area = 1\ or\ 2 \tag{11}$$

$$Kp2_{Area,Min} \leq Kp2_{Area} \leq Kp2_{Area,Max},\ Area = 1\ or\ 2 \tag{12}$$

$$Ki_{Area,Min} \leq Ki_{Area} \leq Ki_{Area,Max},\ Area = 1\ or\ 2 \tag{13}$$

$$n_{Area,Min} \leq n_{Area} \leq n_{Area,Max},\ Area = 1\ or\ 2 \tag{14}$$

The subscripts "min" and "max" represent each region's lowest and highest quantities of each control variable. The comparative amounts are set to be 0 and 3, and the filter parameter n is between 0 and 500 [43].

3. Enhanced Slime Mold Optimization Algorithm

The SMOA offers a unique computing approach that uses dynamic weighting to mimic the mechanisms that cause positive and negative reactions in the slime mold propagating waves to form the optimum path for attaching food [27,34]. The SMOA population is initially generated in the space with dimension (*d*):

$$V_k(0) = V_{\min} + rand(0,1)\cdot[V_{\max} - V_{\min}] \quad k = 1:NK \tag{15}$$

where $V_{\min}$ and $V_{\max}$ represent the minimum and maximum bounds of everyone's control variable, and *NK* is the number of individuals in the population.

Considering that slime mold could follow food based on the fragrance in the air, this behavior may be expressed as follows:

$$V_k(t+1) = \begin{cases} V_b(t) + v_1 \times (W \times V_{r_1}(t) - V_{r_2}(t)) & Pv > r \\ v_2 \times V_k(t) & Pv \leq r \end{cases} \quad k = 1:NK \tag{16}$$

where t represents the current iteration, V_k represents the slime mold position, V_b represents the place having the highest smell concentrations, and V_{r1} and V_{r2} represent two options picked randomly within the population. The slime mold selection behavior is represented by two components, v_1, and v_2, where v_2 decreases linearly from 1 to 0. W is the searching

agent's weight, whereas r is a randomized number between [0, 1]. The Pv formula looks like this:

$$Pv = \tanh|OF(k) - OFB|k = 1 : NK \tag{17}$$

where $OF(k)$ is the current individual's objective rating, OFB is the finest global objective value across the iterations, and v_1: can be represented as follows:

$$v_1 = [-\text{arctanh}\left(1 - \frac{2}{MT}\right), \text{arctanh}\left(1 - \frac{2}{MT}\right)] \tag{18}$$

where MT is the maximal length of iterations. The weight W is as follows:

$$W(Ind_{sm}(k)) = \begin{cases} 1 + r \cdot \log\left(\frac{OFB - OF(k)}{OFB - OFW} + 1\right), & condition \\ 1 + r \cdot \log\left(\frac{OFB - OF(k)}{OFB - OFW} + 1\right), & others \end{cases} \quad k = 1 : NK \tag{19}$$

The first part of the population is represented by *condition*, while r provides a stochastic number between [0, 1]. OFW is the worst objective value obtained in the current iteration, and Ind_{sm} denotes the sorted sequence of objective scores as follows:

$$Ind_{sm} = sort(OF) \tag{20}$$

The second step numerically simulates slime mold venous tissue organization contraction during seeking. The slime mold's seeking activities might vary depending on the kind of food it consumes. The specific technique for altering the placement of the slime mold consists of the following:

$$V_k(t+1) = \begin{cases} V_{\min} + rand(0,1) \times [V_{\max} - V_{\min}] & rand < z \\ V_b(It) + v_1 \times (W \times V_{r_1}(t) - V_{r_2}(t)) & Pv > r \\ v_2 \times V_k(t) & Pv \leq r \end{cases} \tag{21}$$

where $rand$ and r represent arbitrary numbers between 0 and 1. z represents a factor that defines how effectively a matching mechanism would investigate and utilize data, with different values employed depending on the scenario.

Two adjustments have enhanced the SMOA's performance. An enhanced version (ESMOA) with chaotic dynamics and an elite group is used to increase the effectiveness of the original SMOA. An elite group of five members is constructed and refreshed to save the four finest members in every iteration to improve the exploitative seeking function, in addition to the average individual, as follows:

$$V_k(t+1) = V_{Elite}(t) + v_1 \times (W \times V_{r_1}(t) - V_{r_2}(t)) \; if \; Pv > r \tag{22}$$

$$\text{where } V_{Elite}(t) = rand([V_{b1}; V_{b2}; V_{b3}; V_{b4}; V_{Avg}]) \tag{23}$$

As a result, the exploitative-seeking mode is permitted in various desired directions. A logistic mapping with a chaotic tendency is additionally intended to promote the search in a strongly random environment to improve the exploratory seeking characteristic [44]. Depending on it, the chaotic logistic mapping produces a generated vector (Cm) as follows:

$$Cm_k(t+1) = 4Cm_k(t)(Cm_k(t) - 1)) \tag{24}$$

$$\text{where } Cm(0) = rand(1, \dim) \tag{25}$$

According to this approach, that vector is built in each cycle for each control variable. As a result, the standard SMOA upgrading technique has been changed, and the slime mold's new locations have been modified as follows:

$$V_k(t+1) = \begin{cases} V_{\min} + rand(0,1) \times [V_{\max} - V_{\min}] & rand < z \\ Y_{Elitist}(t) + v_1 \times (-V_{r_2}(t) + W \times V_{r_1}(t)) & \Pr > r \\ Cm_k \times v_2 \times V_k(t) & \Pr \leq r \end{cases} \quad (26)$$

Figure 3 depicts the proposed ESMOA's key phases centered on chaotic dynamics and an elite group algorithm.

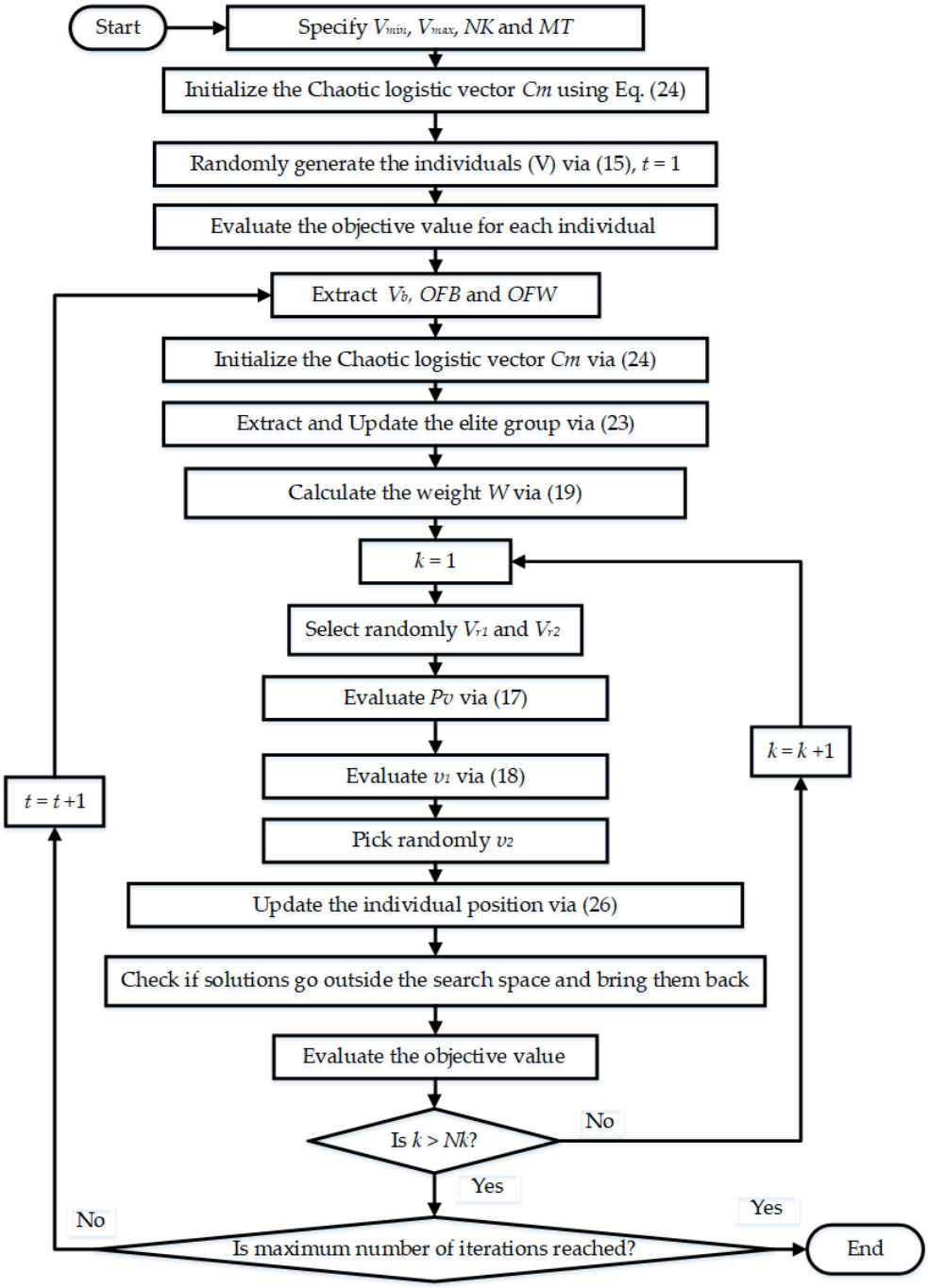

Figure 3. Proposed ESMOA flowchart.

4. Simulation Results and Discussions

This section is divided into two sections. Section 4.1 explores several applications of the proposed ESMOA on different numerical benchmarks compared to the original version of the SMOA. Additionally, the GSO and CO are applied at the same base for examining the comparison with recently applied techniques. Section 4.2 explores the applicability of the proposed ESMOA for the optimal design of cascaded PD-PI controllers for enhancing frequency stability in multi-area power systems.

4.1. Applications on Different Numerical Benchmarks

At first, the proposed ESMOA, the original version of SMOA, GSO, and CO are applied to several applications of the different numerical benchmarks. Because of its incredible complexity, CEC'17 is regarded as a problematic testbed and is, thus, used to evaluate the quality of the suggested ESMOA. The suggested ESMOA is tried on CEC'17 functions with ten dimensions. The CEC'17 test suite consists of 28 standard functions, with F2 removed [45]. It consists of four groups of functions: unimodal (F1 and F3), multi-modal (F4–F10), hybrid (F11–F20), and combination functions. (F21–F29). The capacity to escape local areas is evaluated using multi-modal functions. While composite functions approximating real-world optimization problems with highly dynamic search spaces are used to explore the trade-off regarding the search algorithms' exploitation and exploratory skills. The comparative algorithms are applied with 30 search agents and 500 iterations to guarantee fair comparison. Their convergence features for the 28 benchmark functions are displayed in Figure 4, while their outcomes are tabulated in Tables 1 and 2, respectively, in terms of the best, mean, worst, and standard deviations.

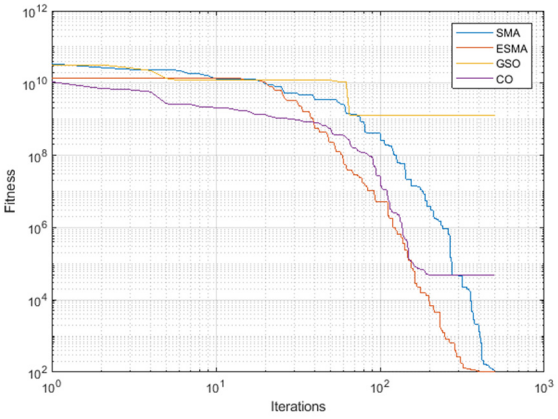

(**a**) F1

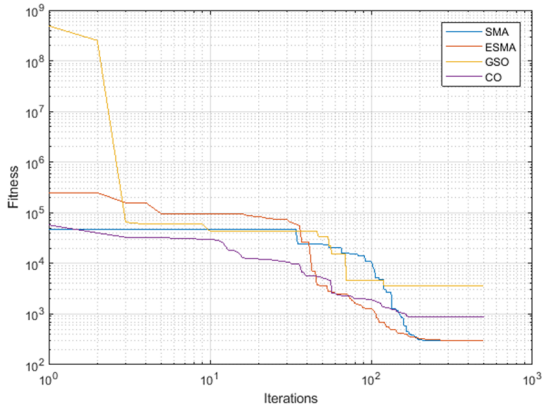

(**b**) F2

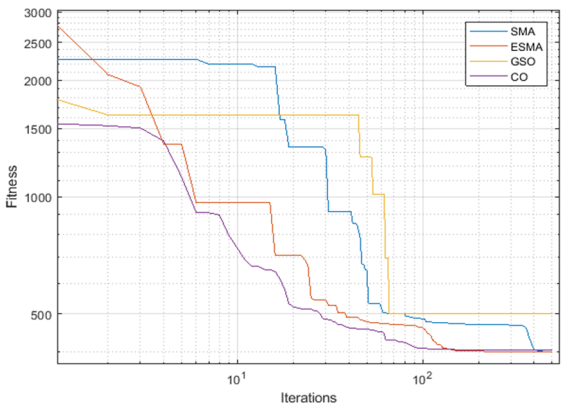

(**c**) F3

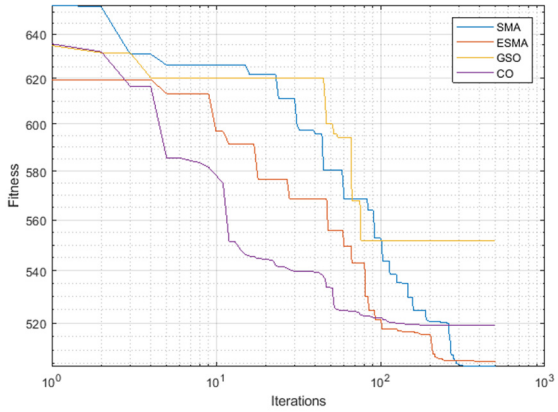

(**d**) F4

Figure 4. *Cont.*

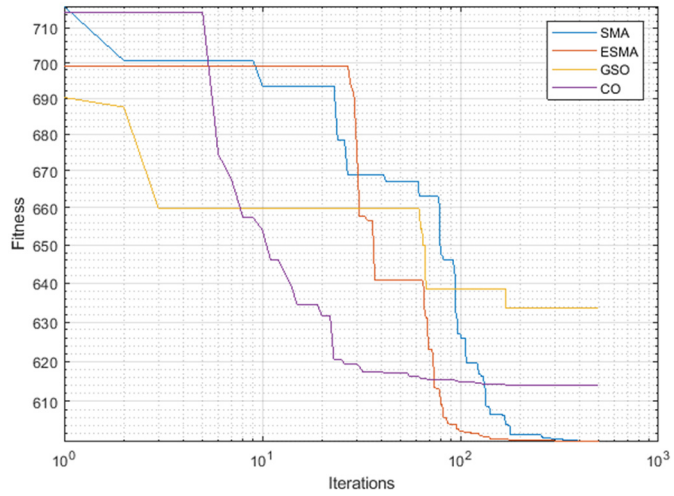

(**e**) F5

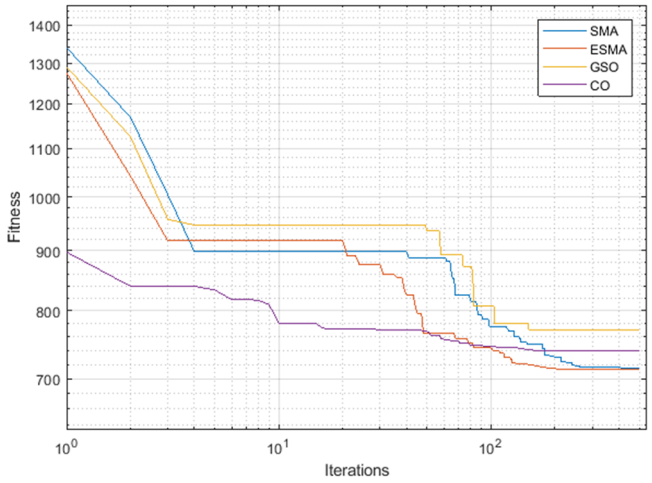

(**f**) F6

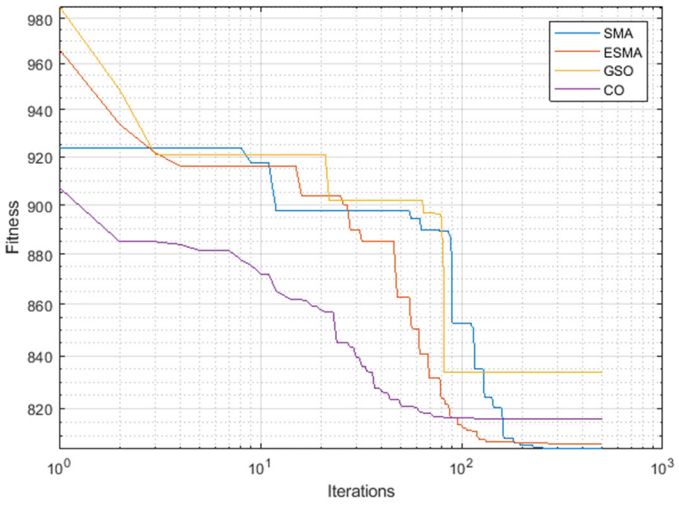

(**g**) F7

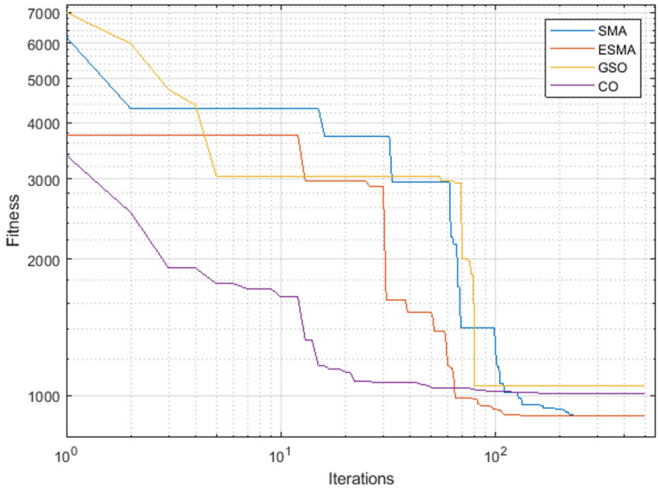

(**h**) F8

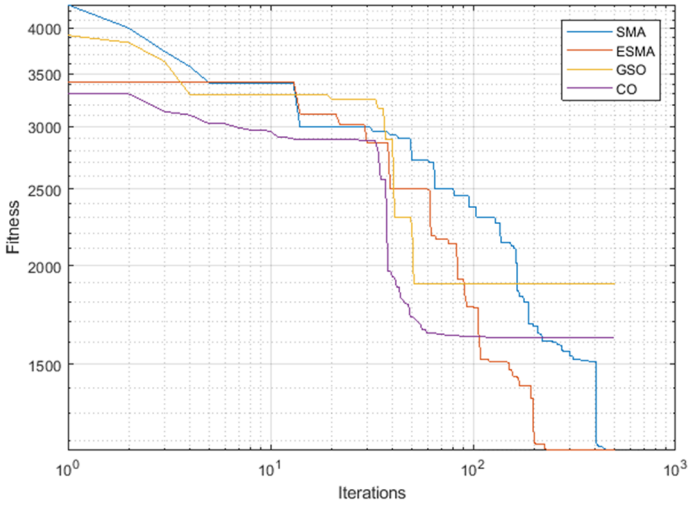

(**i**) F9

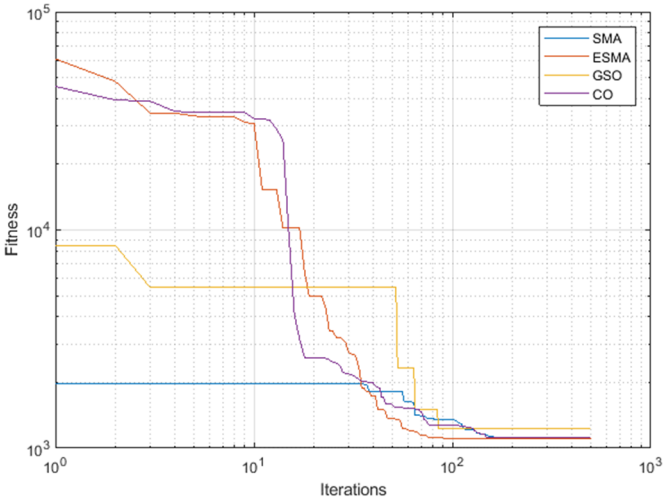

(**j**) F10

Figure 4. *Cont*.

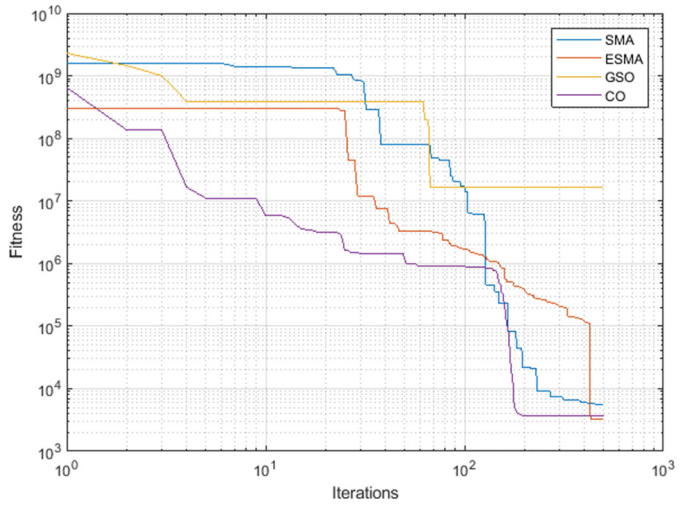

(**k**) F11

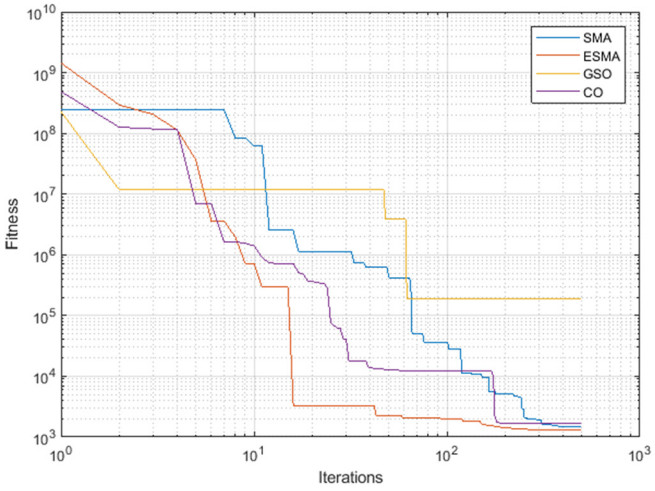

(**l**) F12

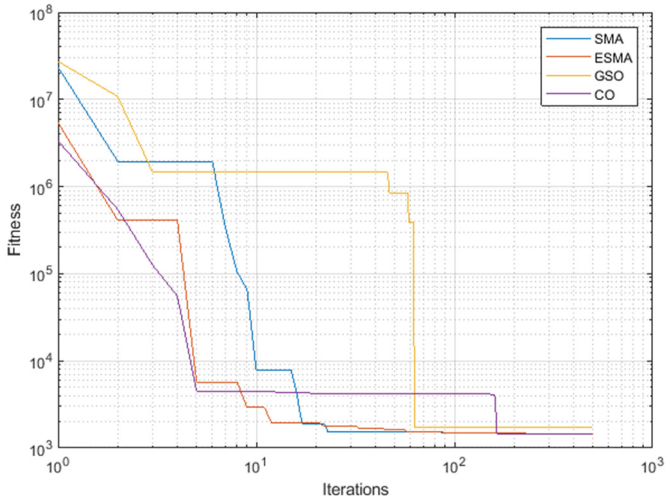

(**m**) F13

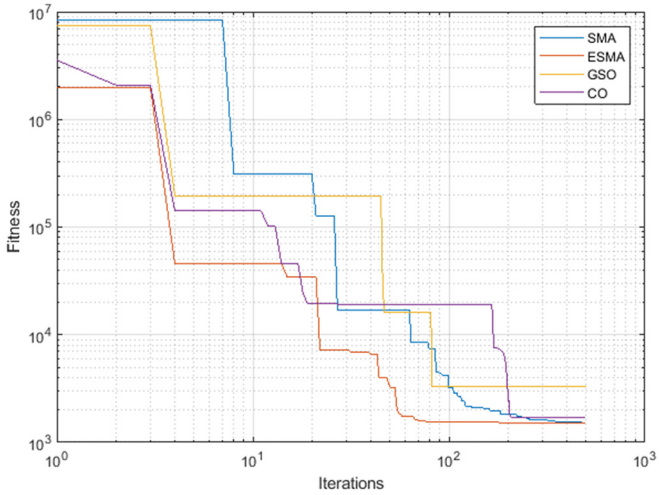

(**n**) F14

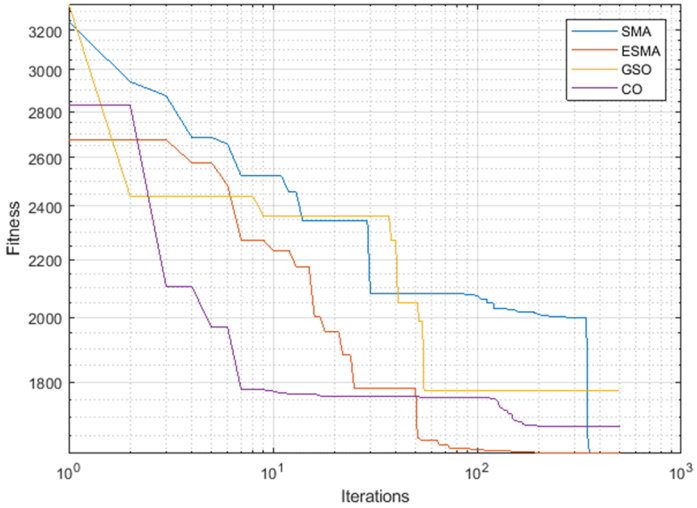

(**o**) F15

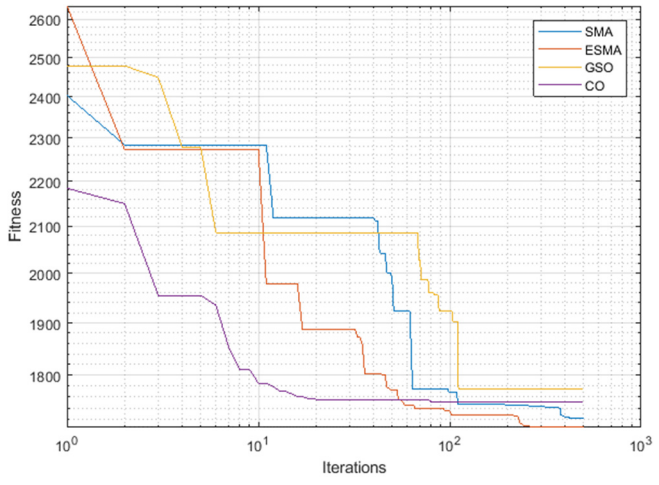

(**p**) F16

Figure 4. *Cont.*

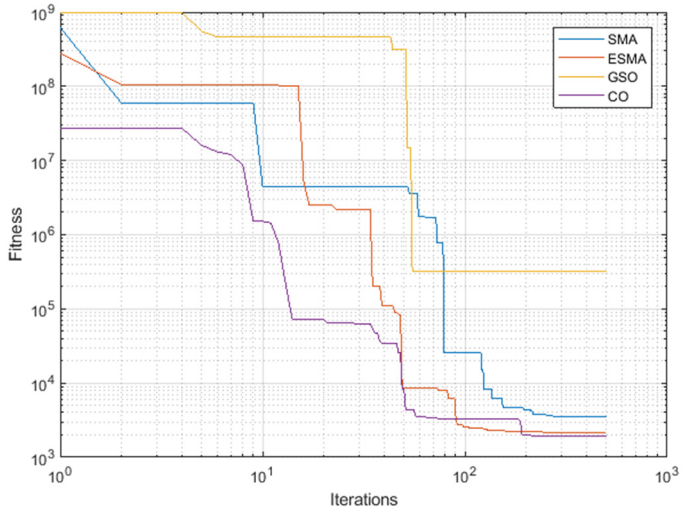

(**q**) F17

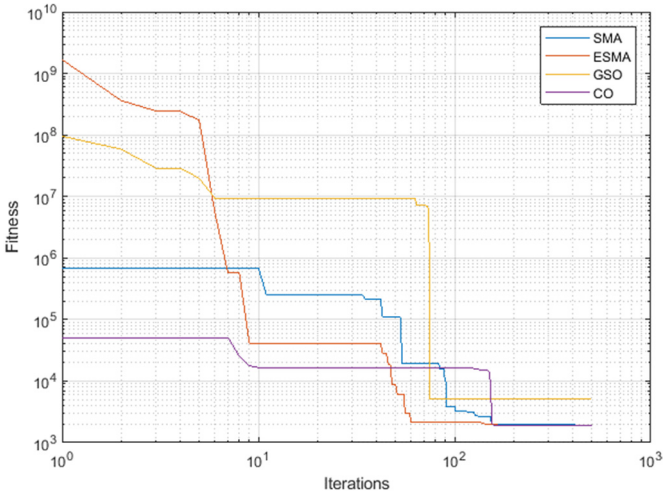

(**r**) F18

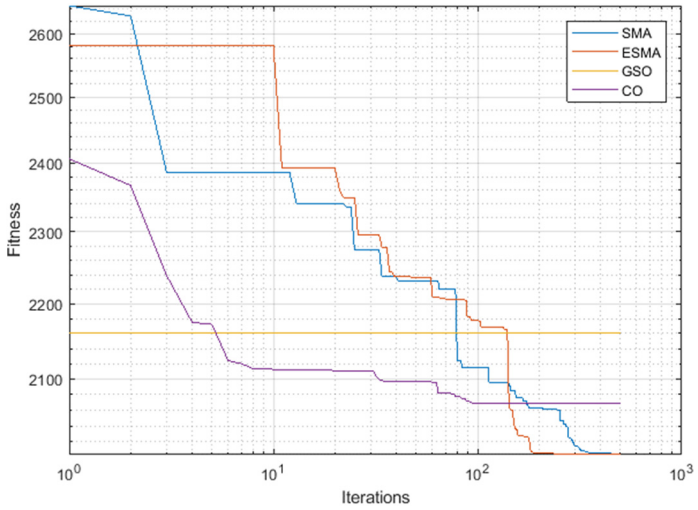

(**s**) F19

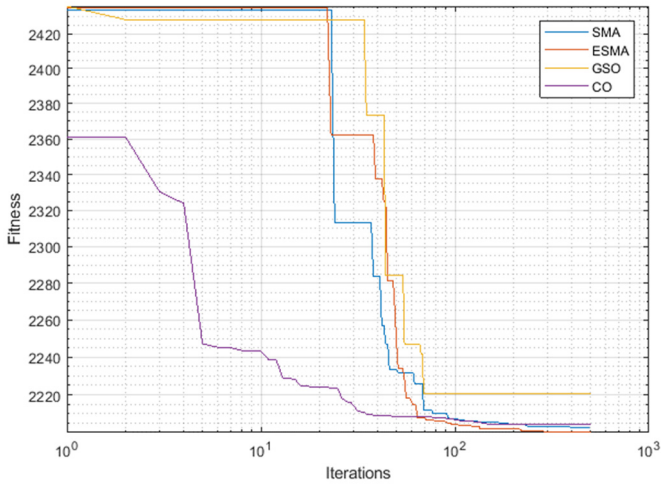

(**t**) F20

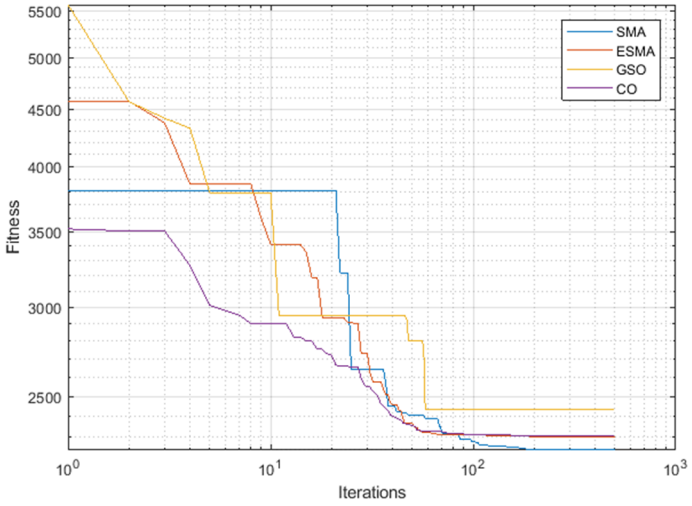

(**u**) F21

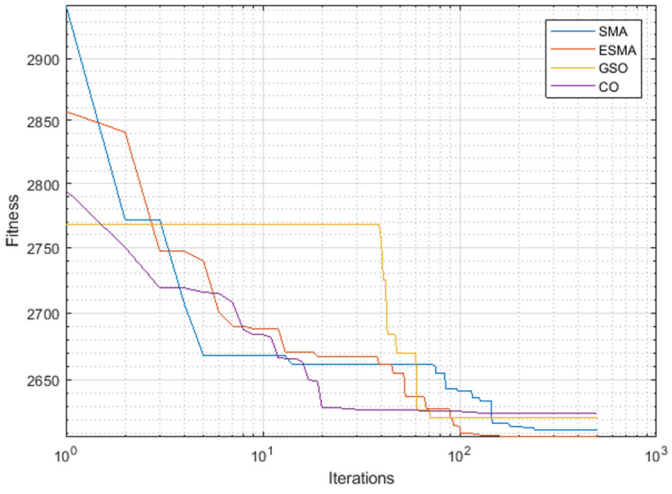

(**v**) F22

Figure 4. *Cont*.

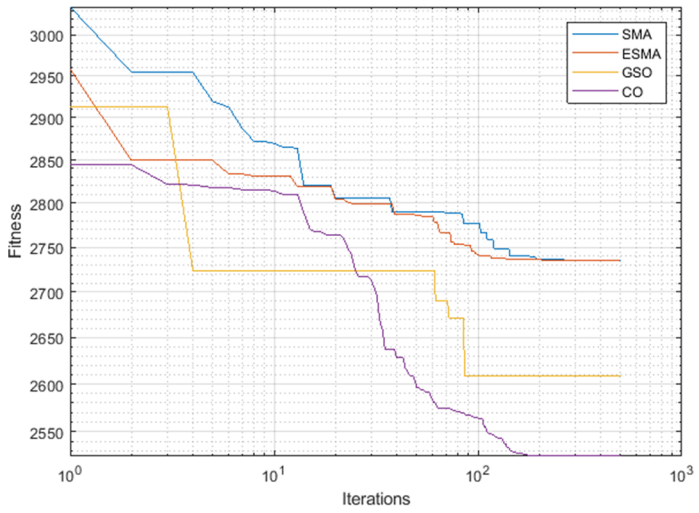

(**w**) F23

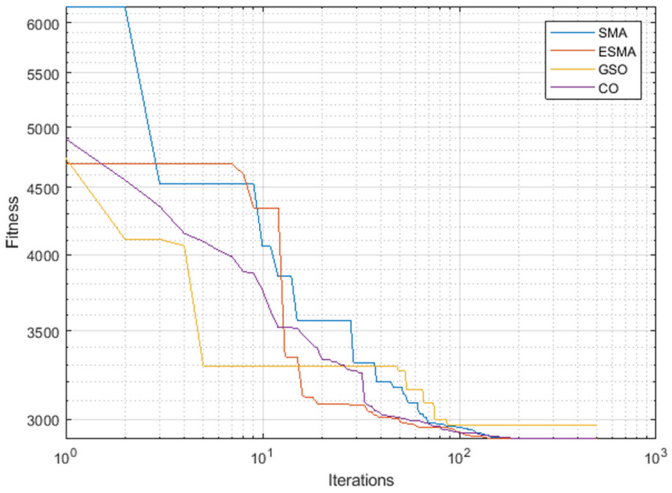

(**x**) F24

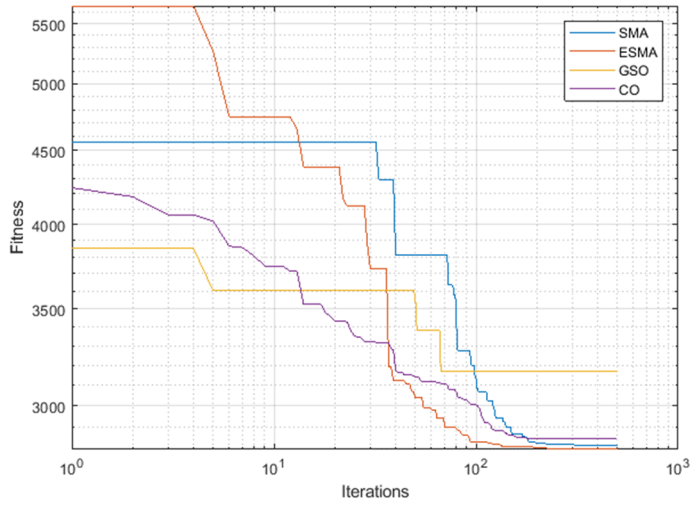

(**y**) F25

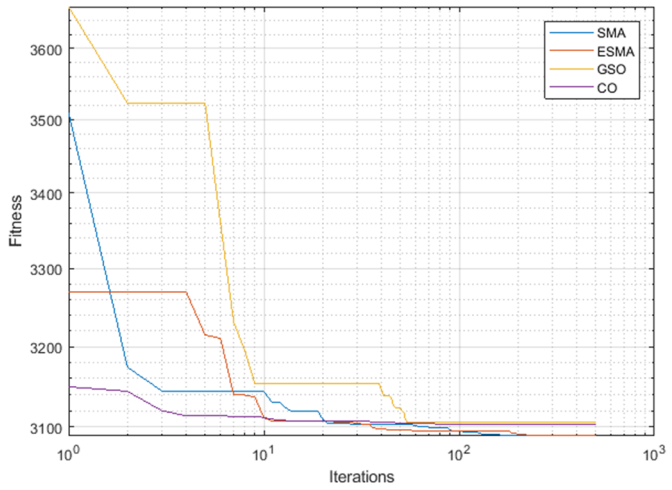

(**z**) F26

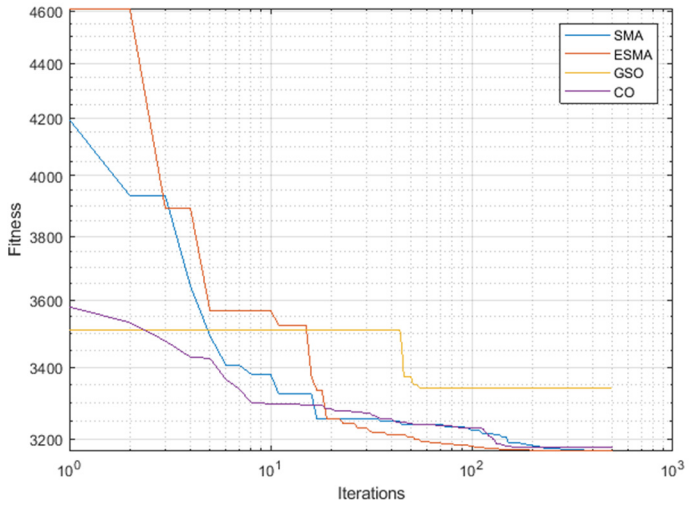

(**aa**) F27

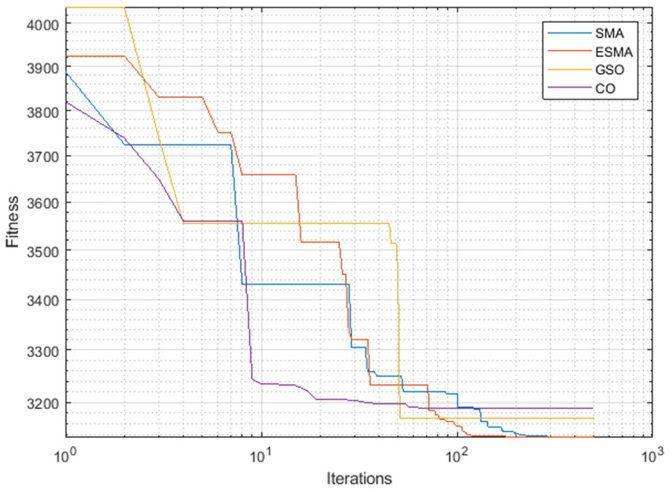

(**ab**) F28

Figure 4. Convergence features of the comparative algorithms for the 28 benchmark functions.

Table 1. Best and mean of the comparative algorithms for the 28 benchmark functions.

Function Name	Best				Mean			
	Proposed ESMOA	Original SMOA	GSO	CO	Proposed ESMOA	Original SMOA	GSO	CO
F1	100.38	115.64	48,532.00	130,840.00	3042.80	4047.10	132,910.00	389,590.00
F2	300.00	300.00	862.84	3631.00	300.09	300.05	14,241.00	7192.00
F3	400.01	400.05	404.19	501.24	405.41	407.54	506.25	714.73
F4	505.97	503.98	519.12	551.75	515.62	514.89	561.92	579.45
F5	600.04	600.08	614.06	633.65	600.09	600.17	645.26	646.92
F6	712.85	715.20	739.97	771.23	724.81	725.50	789.00	796.06
F7	806.97	804.98	816.01	833.54	814.53	816.62	846.86	850.81
F8	900.00	900.00	1007.40	1049.20	900.00	900.25	1631.00	1403.00
F9	1165.30	1168.70	1621.20	1898.30	1462.20	1511.80	2610.20	2727.50
F10	1101.00	1103.40	1116.00	1233.00	1112.40	1137.80	2006.00	1659.30
F11	3253.40	5561.40	3612.70	1,662,800.00	21,345.00	207,930.00	248,790.00	131,410.00
F12	1319.60	1465.10	1679.70	190,570.00	2161.80	8132.90	108,430.00	329,250.00
F13	1434.10	1435.00	1446.60	1740.20	1764.30	1929.00	3889.00	5668.90
F14	1504.70	1522.30	1713.10	3271.00	4320.80	3349.90	18,439.00	11,877.00
F15	1601.80	1602.10	1675.80	1775.30	1646.50	1663.50	2083.80	2070.70
F16	1705.50	1721.00	1750.60	1774.90	1730.10	1747.10	1889.90	1811.90
F17	2166.90	3473.40	1949.00	326,110.00	24,256.00	19,428.00	502,870.00	75,619.00
F18	1915.70	1908.00	1935.80	5104.50	3553.30	5501.10	726,860.00	229,180.00
F19	2004.00	2005.30	2068.10	2161.40	2021.80	2030.30	2268.90	2250.60
F20	2200.00	2202.80	2204.60	2220.40	2313.90	2304.40	2341.70	2329.20
F21	2300.50	2241.00	2308.10	2436.00	2301.90	2298.10	2417.30	2632.50
F22	2607.40	2612.40	2625.10	2621.30	2616.50	2619.50	2718.90	2687.20
F23	2735.40	2734.70	2524.40	2608.40	2751.00	2751.60	2822.50	2792.70
F24	2897.80	2898.20	2901.50	2971.10	2917.80	2922.20	2971.40	3155.50
F25	2800.20	2816.00	2848.80	3166.90	2953.30	3022.60	3667.10	3494.10
F26	3089.00	3089.00	3103.70	3105.40	3091.00	3090.50	3174.10	3154.90
F27	3166.50	3167.50	3176.30	3341.20	3342.20	3320.00	3478.50	3587.20
F28	3134.40	3134.40	3189.20	3171.20	3180.70	3186.20	3384.80	3422.50

From both tables, the proposed ESMOA shows great effectiveness and robustness over the original SMOA, GSO, and CO. Compared to the original SMOA, the proposed ESMOA shows superiority in 78.57%, 67.86%, 96.43%, and 96.43% of the benchmark functions regarding the best, mean, worst, and standard deviations of the obtained fitness. Compared to the GSO, the proposed ESMOA shows superiority in 92.86%, 100%, 100%, and 100% of the benchmark functions regarding the best, mean, worst, and standard deviations of the obtained fitness. Compared to the CO, the proposed ESMOA shows superiority in 96.43%, 100%, 100%, and 100% of the benchmark functions regarding the best, mean, worst, and standard deviations of the obtained fitness.

Table 2. Worst and standard deviations of the comparative algorithms for the 28 benchmark functions.

Function Name	Worst				Standard Deviation			
	Proposed ESMOA	Original SMOA	GSO	CO	Proposed ESMOA	Original SMOA	GSO	CO
F1	5542.40	12,677.00	28,897.00	92,394.00	1949.30	3400.70	44,212.00	14,445.00
F2	300.39	300.35	78,883.00	10,628.00	0.09	0.08	17,009.00	1924.90
F3	407.21	456.99	1547.10	1006.70	2.11	9.52	190.61	106.96
F4	521.49	530.26	623.22	611.50	3.88	6.32	27.66	11.15
F5	600.12	600.51	678.05	662.27	0.02	0.09	14.44	7.06
F6	731.80	742.81	880.06	818.59	5.11	6.82	29.91	10.39
F7	820.90	829.85	923.48	863.56	4.19	5.58	21.18	5.72
F8	900.00	905.83	4350.50	1677.10	0.00	1.07	577.21	154.49
F9	1679.00	1980.10	3664.50	3020.80	146.27	196.82	486.29	246.06
F10	1124.30	1336.50	17,767.00	3062.20	6.67	62.63	2411.60	352.41
F11	597,810.00	1,267,400.00	2,418,100.00	2,363,500.00	18,966.00	31,202.00	57,591.00	595,460.00
F12	4041.90	32,548.00	270,800.00	186,570.00	647.76	10,628.00	53,603.00	38,638.00
F13	2504.00	8381.60	28,906.00	29,799.00	326.27	1330.90	7451.90	5085.40
F14	7356.10	11,424.00	103,090.00	20,748.00	1898.70	2415.70	25,557.00	3936.90
F15	1731.60	1899.60	2769.80	2283.20	45.34	73.85	226.49	98.50
F16	1747.80	1838.80	2217.90	1850.10	12.03	25.04	107.15	17.22
F17	35,618.00	42,539.00	125,660.00	255,060.00	9720.00	11,108.00	248,740.00	71,446.00
F18	13,985.00	28,127.00	198,640.00	973,510.00	2695.90	7991.50	31,346.00	25,352.00
F19	2036.50	2073.60	2693.20	2386.00	10.30	14.61	117.47	40.63
F20	2328.90	2335.40	2413.90	2413.70	31.07	40.63	53.19	59.64
F21	2302.90	2304.20	3791.10	2979.90	0.65	14.43	246.41	108.66
F22	2623.60	2633.50	2901.10	2755.20	4.60	5.06	56.51	20.75
F23	2762.70	2772.20	2992.40	2923.00	7.40	8.60	97.58	51.44
F24	2947.00	2969.40	3179.20	3382.30	23.58	25.47	56.40	81.43
F25	2999.10	3920.70	4859.70	4128.60	46.95	289.78	582.65	206.69
F26	3092.70	3095.30	3312.60	3219.60	1.18	1.48	50.31	37.80
F27	3411.80	3731.80	4019.00	3750.10	102.46	137.11	212.66	120.79
F28	3235.30	3283.50	3757.00	3663.20	32.19	38.54	135.63	97.90

4.2. Applications for Enhancing Frequency Stability in Multi-Area Power Systems

In this part, the suggested ESMOA (Figure 3) is utilized to minimize the goal function of ITAE, which is specified in Equation (8). The GSO and CO procedures are also employed for comparison. The number of iterations is set to 100, while the number of search agents is 10. Four separate testing cases are run, each having distinct perturbations. The whole simulation process is carried out in MATLAB. The data from the understudied MAPSs are similar to those from the references [17,46]. All tests are run with the same number of function repetitions to provide a fair comparison of the competing approaches. As noted, four instances are explored based on the positioning of the step change:

- Case 1: Step load disturbance only in area 1.
- Case 2: Step load disturbance only in area 2.
- Case 3: Step load disturbance in areas 1 and 2.

- Case 4: Step load disturbance only in area 1 considering non-linearities in the power system.

4.2.1. Application for Case 1

Area 2 remains unaltered in this case, but a 0.1 p.u step load augmentation hike in area 1 is assessed. The suggested ESMOA (Figure 3), GSO, and CO techniques are applied; Figure 5 shows the corresponding converging characteristics, and Table 3 summarizes the simulated data for the investigated ITAE minimizing approaches. The summarized data accompany the ITAE target scores and the related parameter settings of K_{p1}, K_i, K_{p2}, K_d, and n in each area. As shown, the proposed ESMOA achieves the lowest value regarding the ITAE objective of 0.023431, where GSO and CO obtain ITAE objective values of 0.023922 and 0.02677, respectively.

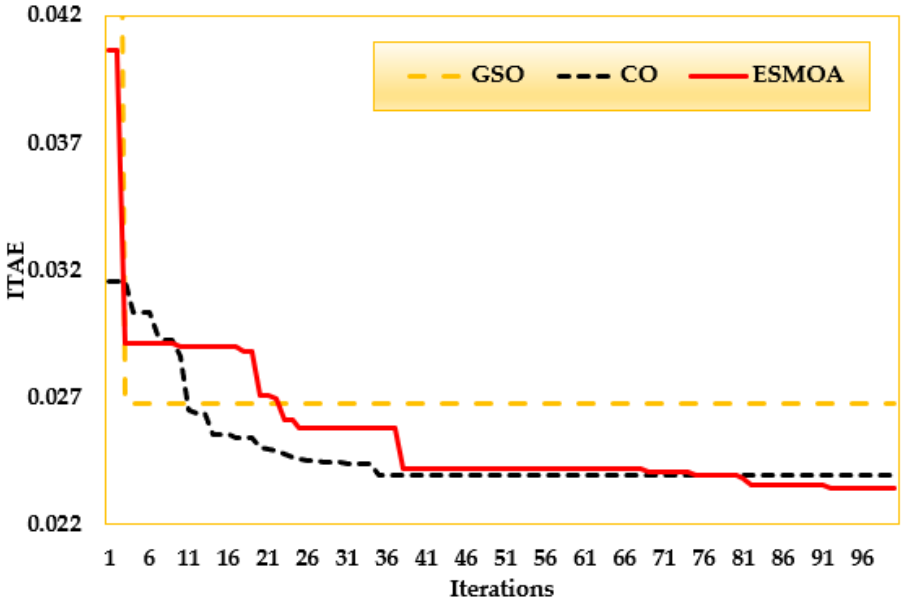

Figure 5. Converging characteristics of the suggested ESMOA, GSO, and CO techniques for Case 1.

Table 3. Results for Case 1.

Algorithm			Proposed ESMOA	GSO	CO
Controller parameters	K_{P1}	Area 1	3	3	3
	K_i		1.198019018	1.882598713	1.125704786
	K_{P2}		3	3	3
	K_d		1.575698137	1.163053801	1.712103293
	n		500	198.3903318	500
	K_{P1}	Area 2	0.167226621	3	2.477149042
	K_i		0.88462493	1.597201322	2.639381164
	K_{P2}		2.881063135	0.731447135	3
	K_d		3	2.903096059	2.095134679
	n		392.6175818	40.09581819	283.8518794
ITAE Value			0.023431548	0.026772795	0.023922459
ITAE improvement percent compared to the proposed ESMOA			-	12.48	2.0521

Figure 6 also shows the dynamic responses for frequency variations in each region and tie-line transfer power. As seen in Figure 6, the suggested ESMOA outperforms the CO and GSO in reducing the objective function. Even though the GSO algorithm delivers the quickest reaction when approaching the stable region, multiple oscillations are present, particularly in the frequency deviation in area 2.

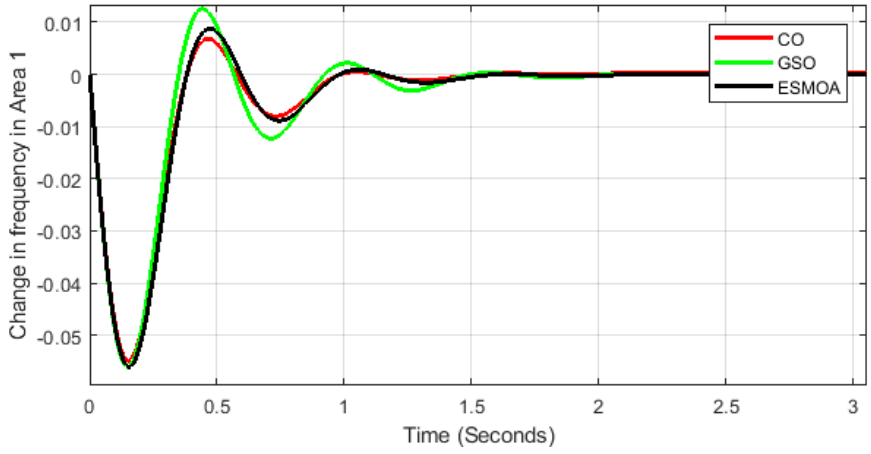

(**a**)

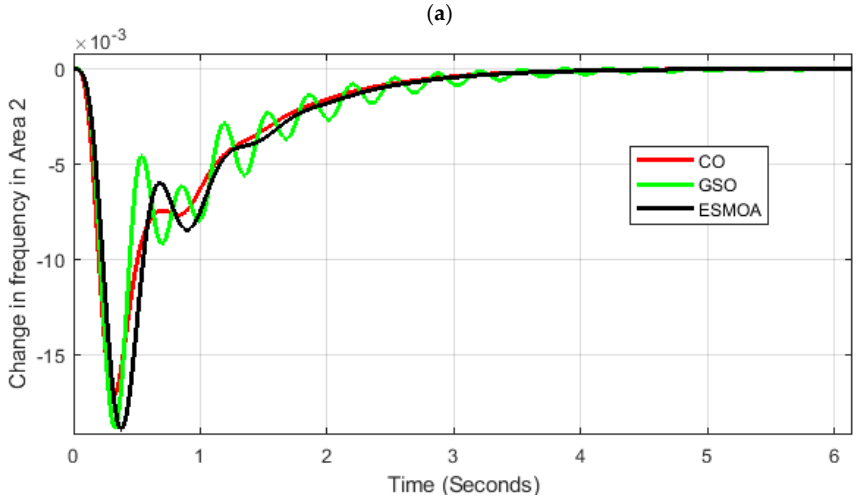

(**b**)

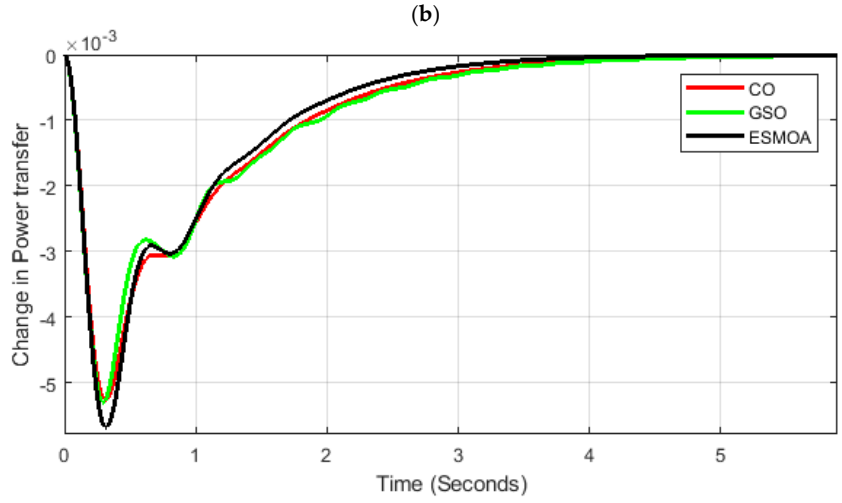

(**c**)

Figure 6. Dynamic responses for CO, GSO, and the proposed ESMOA for Case 1. (**a**) Deviation in frequency in area 1. (**b**) Deviation in frequency in area 2. (**c**) Deviation in transferred power through interconnected tie-line.

From the reported results, the ESMOA algorithm gives a slightly smaller ITAE value (0.023431548) compared with that given by the GSO (0.026772795). The decreased amount represents 12.486% which declares a significant improvement percentage in this case. On the other side, as shown in Figure 6, the corresponding outputs are reasonably coincident regarding the change in frequency in area 1 (Figure 6a). However, slight improvement is shown in the change in frequency in area 2 (Figure 6b). At the same time, significant mitigation is declared regarding the change in power transfer between the two areas (Figure 6c).

Figure 7 depicts the assessed four measures of the lowest, mean, maximum, and standard deviation produced by ITAE throughout several independent operations to provide statistical comparability between CO, GSO, and the suggested ESMOA. This figure states the recommended ESMOA's high efficacy and capability compared to CO and GSO. The suggested ESMOA is used to obtain the smallest measurements, as illustrated. It finds the smallest minimum, mean, maximum, and standard deviation with 0.023431548, 0.024266891, 0.02780845, and 0.001298062, respectively.

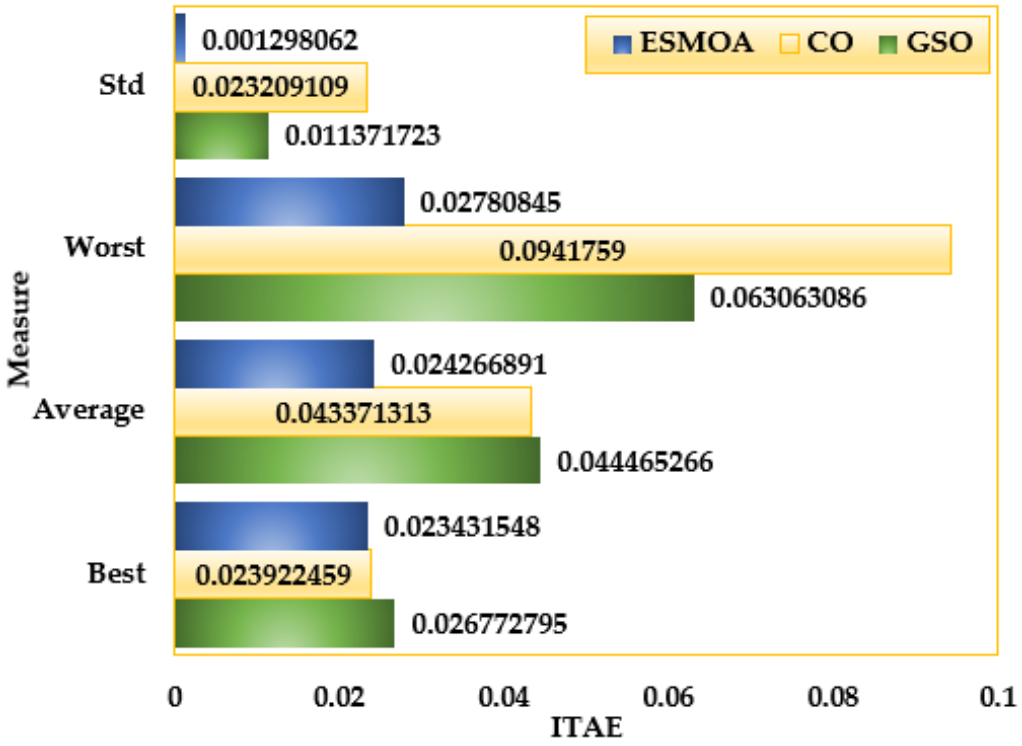

Figure 7. Statistical measures for CO, GSO, and the proposed ESMOA for Case 1.

Table 4 contrasts the efficacy of the proposed ESMOA-based PD-PI controller with various previously published controlling methods concerning ITAE and settling time. As shown, the proposed ESMOA-based PD-PI controller obtains the minimum ITAE of 0.02343 where the conventional PI, PI-based-BFOA, PI-based-DE, PI-based-BFOA-PSO, PI-based-GA, PI-based-FA, PI-based-PSO, PID-based-ARA, PI-based-FA, CO-based PD-PI controller, and GSO-based PD-PI controller find 3.5795, 1.8379, 0.9911, 1.1865, 2.7475, 0.8695, 1.2142, 0.075401, 0.4714, 0.02392, and 0.02677, respectively. Regarding the lowest ITAE value, frequency settling time, and tie-line power variations, the proposed ESMOA-based PD-PI controller beats the other previously published optimization strategies, as shown in the table.

Table 4. Comparison of the proposed ESMOA outcomes with other reported results in terms of ITAE and settling time.

Controller	Optimization Technique	Reference	Settling Times (s)			Objective Value
			ΔP_{TIE}	ΔF_2	ΔF_1	ITAE
PI	Conventional	[46]	28.270	45.010	45.00	3.5795
PI	BFOA	[46]	6.350	7.090	5.520	1.8379
PI	DE	[17]	5.750	8.160	8.960	0.9911
PI	BFOA-PSO	[19]	5.730	7.650	7.390	1.1865
PI	GA	[46]	9.370	11.390	10.590	2.7475
PI	Firefly algorithm (FA)	[46]	5.620	7.220	7.110	0.8695
PI	PSO	[19]	5.000	7.820	7.370	1.2142
PID	Artificial rabbits' algorithm (ARA)	[40]	3.059294	2.901341	2.195834	0.075401
PID	FA	[46]	4.780	5.490	4.250	0.4714
PD-PI	CO	Applied	3.8157	3.1087	1.3395	0.023922459
PD-PI	GSO	Applied	3.9883	3.7314	1.4118	0.026772795
PD-PI	Proposed ESMOA	Applied	3.3018	3.1172	1.4202	0.023431548

4.2.2. Application for Case 2

Area 1 remains unaltered in this case, but a 0.1 p.u step load augmentation hike in area 2 is assessed. The suggested ESMOA, GSO, and CO techniques are applied; Figure 8 shows the corresponding converging characteristics, and Table 5 summarizes the simulated data for the investigated ITAE minimizing approaches. The summarized data accompany the ITAE target scores and the related parameter settings of K_{p1}, K_i, K_{p2}, K_d, and n in each area. As shown, the proposed ESMOA achieves the lowest ITAE objective value of 0.023653, where CO and GSO obtain ITAE objective values of 0.023821 and 0.026281, respectively. Therefore, the suggested ESMOA improves the ITAE value by 10% compared to GSO and 0.71% compared to CO.

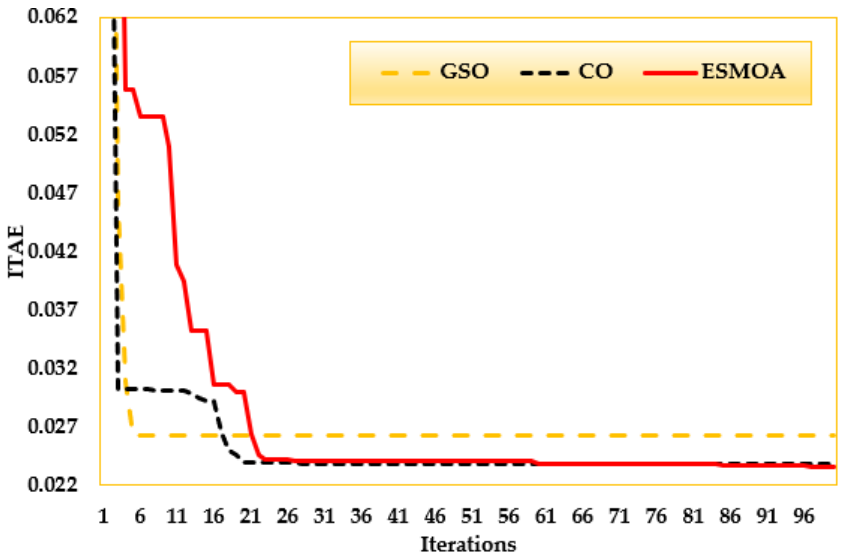

Figure 8. Converging characteristics of the suggested ESMOA, GSO, and CO techniques for Case 2.

Table 5. Results for Case 2.

Algorithm			Proposed ESMOA	GSO	CO
Controller parameters	K_{P1}	Area 1	3	3	3
	K_i		2.712281	3	3
	K_{P2}		0.019315	3	3
	K_d		1.315795	1.217712	2.178291
	n		336.0855	282.2859	500
	K_{P1}	Area 2	3	3	3
	K_i		1.174453	1.893716	1.244513
	K_{P2}		3	3	3
	K_d		1.644572	1.373006	1.585313
	n		489.4933	183.442	471.6436
ITAE Value			0.023653	0.026281	0.023821
ITAE improvement percent compared to the proposed ESMOA			-	9.99	0.7057

Figure 9 also shows the dynamic responses for frequency variations in each region and tie-line transfer power. As seen in Figure 9, the suggested ESMOA outperforms the CO and GSO in reducing the objective function. It provides the lowest settling times of 3.0999, 0.92, and 3.6663 s for the deviations in frequency in area 1, frequency in area 2, and transfer power, respectively. The CO algorithm obtains settling times of 3.1744, 1.3345, and 3.7474 s, while the GSO algorithm attains settling times of 3.5335, 1.5755, and 4.2202 s for the deviations in frequency in area 1, frequency in area 2, and transfer power, respectively.

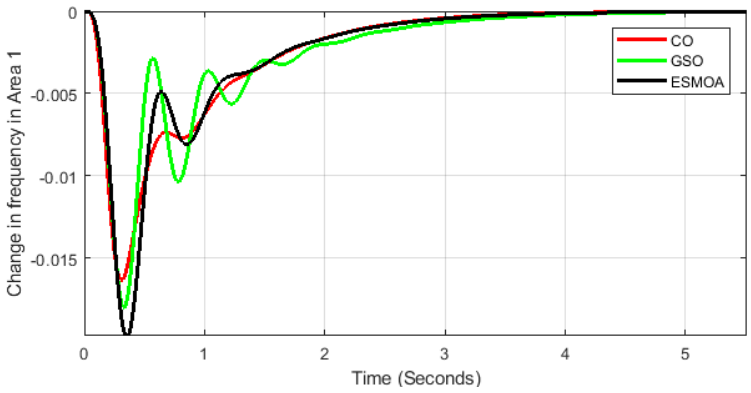

(**a**)

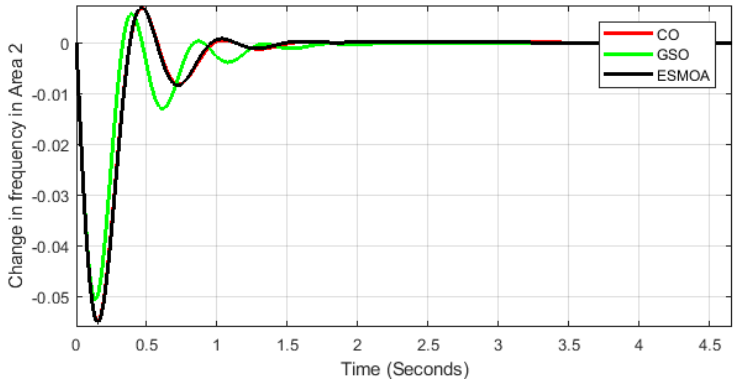

(**b**)

Figure 9. *Cont.*

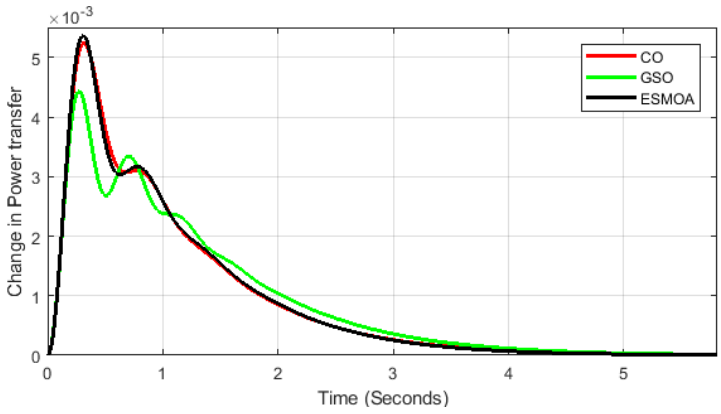

(**c**)

Figure 9. Dynamic responses for CO, GSO, and the proposed ESMOA for Case 2. (**a**) Deviation in frequency in area 1. (**b**) Deviation in frequency in area 2. (**c**) Deviation in transferred power through interconnected tie-line.

For this case, Figure 10 depicts the assessed four measures of the lowest, mean, maximum, and standard deviation of the produced ITAE throughout several independent operations to provide statistical comparability between CO, GSO, and the suggested ESMOA. The suggested ESMOA is used to obtain the smallest measurements, as illustrated. It finds the smallest minimum, mean, maximum, and standard deviation with 0.023653, 0.02491, 0.027762, and 0.001483, respectively.

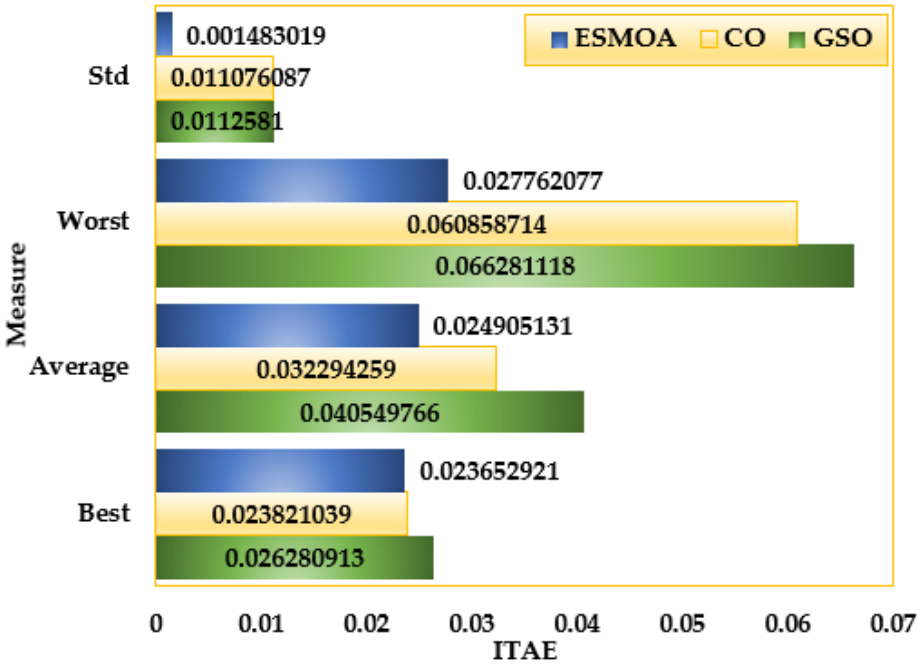

Figure 10. Statistical measures for CO, GSO, and the proposed ESMOA for Case 2.

Table 6 contrasts the efficacy of the proposed ESMOA-based PD-PI controller with various previously published controlling methods concerning ITAE. As shown, the proposed ESMOA-based PD-PI controller obtains the minimum ITAE of 0.023653, while the conventional PID-based-PSO, PID-based-ARA, PID-based-JAYA, PI-based-DE, PID-based-SAMPE-JAYA, CO-based PD-PI controller, and GSO-based PD-PI controller find 0.0816, 0.075409, 0.078, 0.082, 0.077, 0.023821, and 0.026281, respectively.

Table 6. Comparison of the proposed ESMOA outcomes with other reported results in terms of ITAE for Case 2.

Controller	Optimization Technique	Reference	ITAE Objective Value
PID	PSO	[40]	0.0816
PID	ARA	[40]	0.075409
PID	JAYA	[40]	0.078
PID	DE	[40]	0.082
PID	SAMPE-JAYA	[40]	0.077
PD-PI	CO	Applied	0.023821
PD-PI	GSO	Applied	0.026281
PD-PI	Proposed ESMOA	Applied	0.023653

4.2.3. Application for Case 3

In areas 1 and 2, a simultaneous 0.1 p.u. step load augmentation hike is assessed for this case. The suggested ESMOA, GSO, and CO techniques are applied; Figure 11 shows the corresponding converging characteristics, and Table 7 summarizes the simulated data for the investigated ITAE minimizing approaches. The summarized data accompany the ITAE target scores and the related parameter settings of K_{p1}, K_i, K_{p2}, K_d, and n in each area. As shown, the proposed ESMOA achieves the lowest ITAE objective value of 0.04428, while CO and GSO obtain ITAE objective values of 0.075148 and 0.08294, respectively. Therefore, the suggested ESMOA improves the ITAE value by 41.1% compared to GSO and 46.61% compared to CO.

Figure 12 also shows the dynamic responses for frequency variations in each region and tie-line transfer power. The suggested ESMOA outperforms the CO and GSO in reducing the objective function. It provides the lowest settling times of 2.5137, 1.5619, and 3.5789 s for the deviations in frequency in areas 1 and 2 and the transfer power, respectively. The CO algorithm obtains settling times of 3.62, 2.2824, and 5.2696 s. In contrast, the GSO algorithm attains settling times of 4.0042, 3.227, and 4.9151 s for the deviations in frequency in area 1, frequency in area 2, and transfer power, respectively.

Table 7. Results for Case 3.

Algorithm			Proposed ESMOA	GSO	CO
Controller parameters	K_{P1}	Area 1	3	3	3
	K_i		1.080022	3	0.719087
	K_{P2}		3	3	3
	K_d		1.424285	0.908199	2.467428
	n		448.7811	202.1082	38.15772
	K_{P1}	Area 2	3	3	2.904342
	K_i		1.05636	3	0.56298
	K_{P2}		3	3	2.893778
	K_d		1.551031	0.908199	3
	n		474.3045	202.1082	500
ITAE Value			0.044279	0.082937	0.075148
ITAE improvement percent compared to the proposed ESMOA			-	46.611	41.0773

For this case, Figure 13 depicts the assessed four measures of the lowest, mean, maximum, and standard deviation of the produced ITAE throughout several independent operations to provide statistical comparability between CO, GSO, and the suggested ESMOA. The suggested ESMOA is used to obtain the smallest measurements, as illustrated. It finds the smallest minimum, mean, maximum, and standard deviation with 0.044279, 0.04573, 0.04841, and 0.001272, respectively.

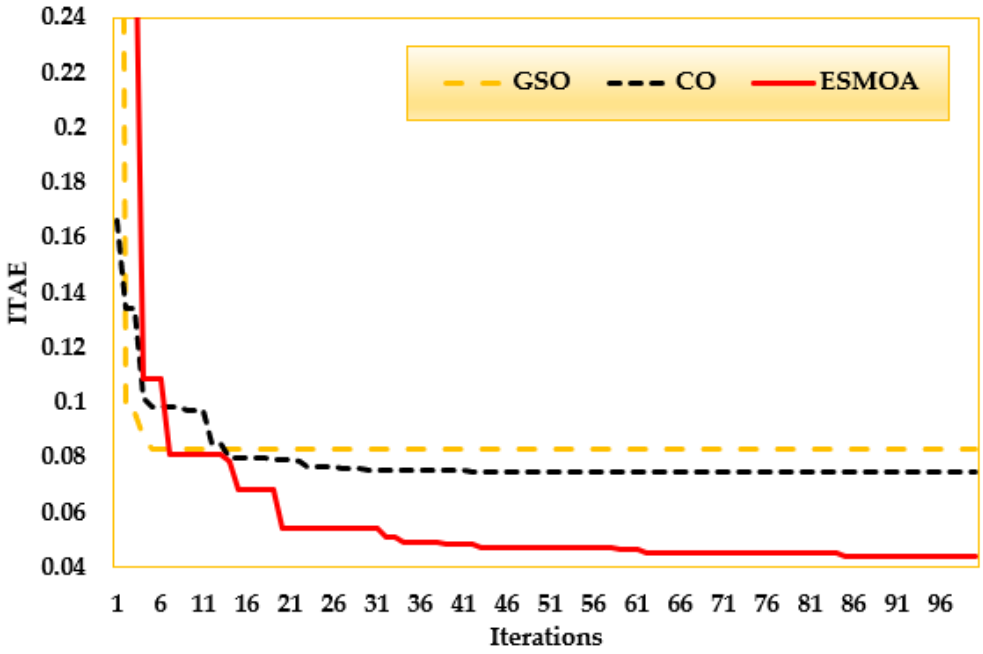

Figure 11. Converging characteristics of the suggested ESMOA, GSO, and CO techniques for Case 3.

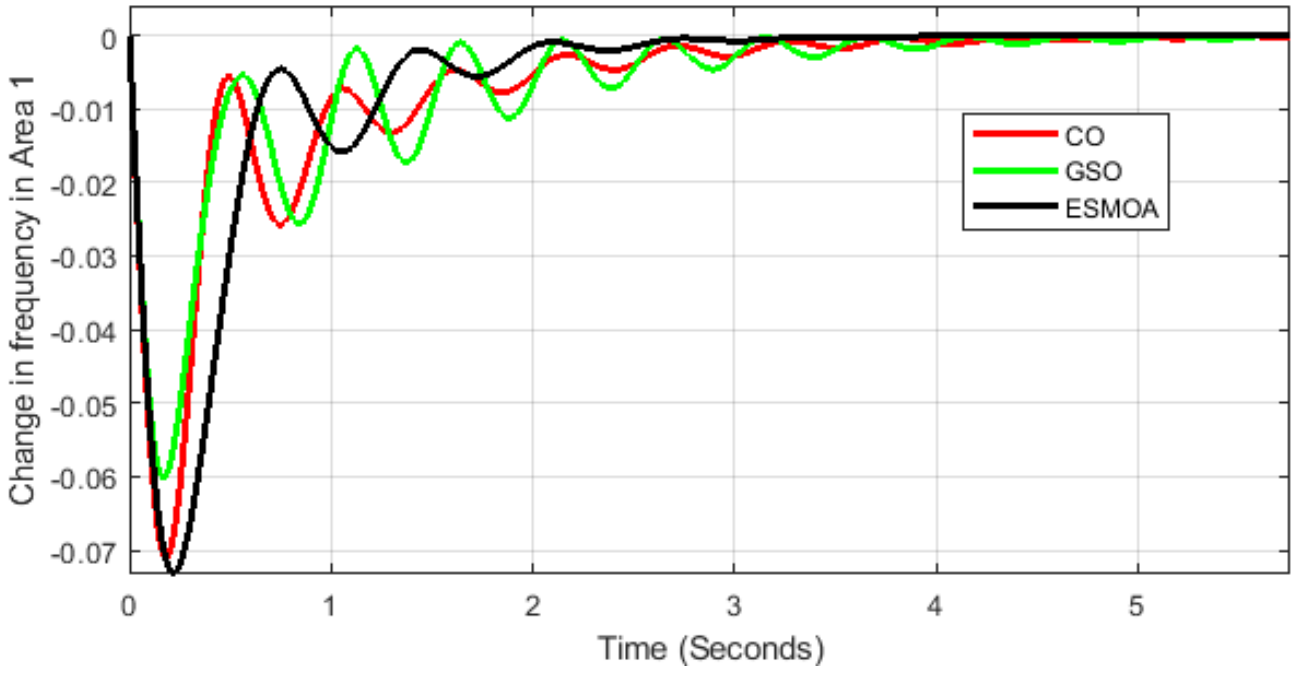

(**a**)

Figure 12. *Cont.*

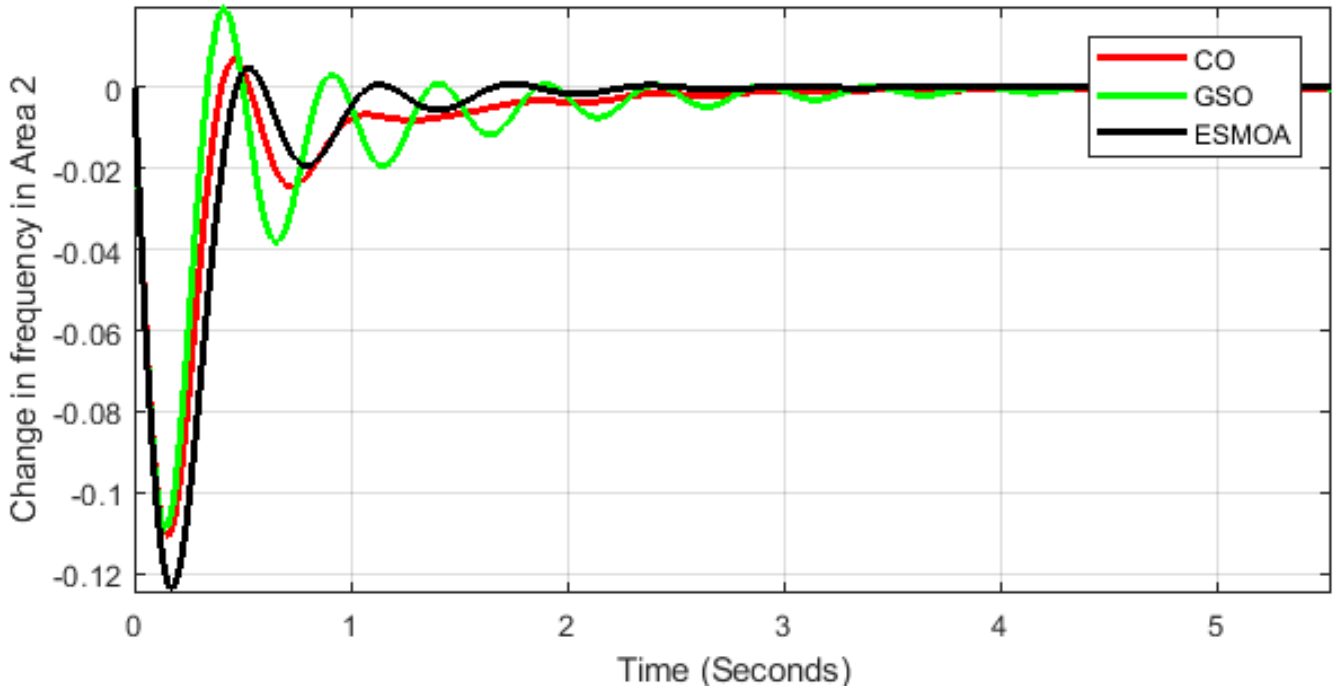

(**b**)

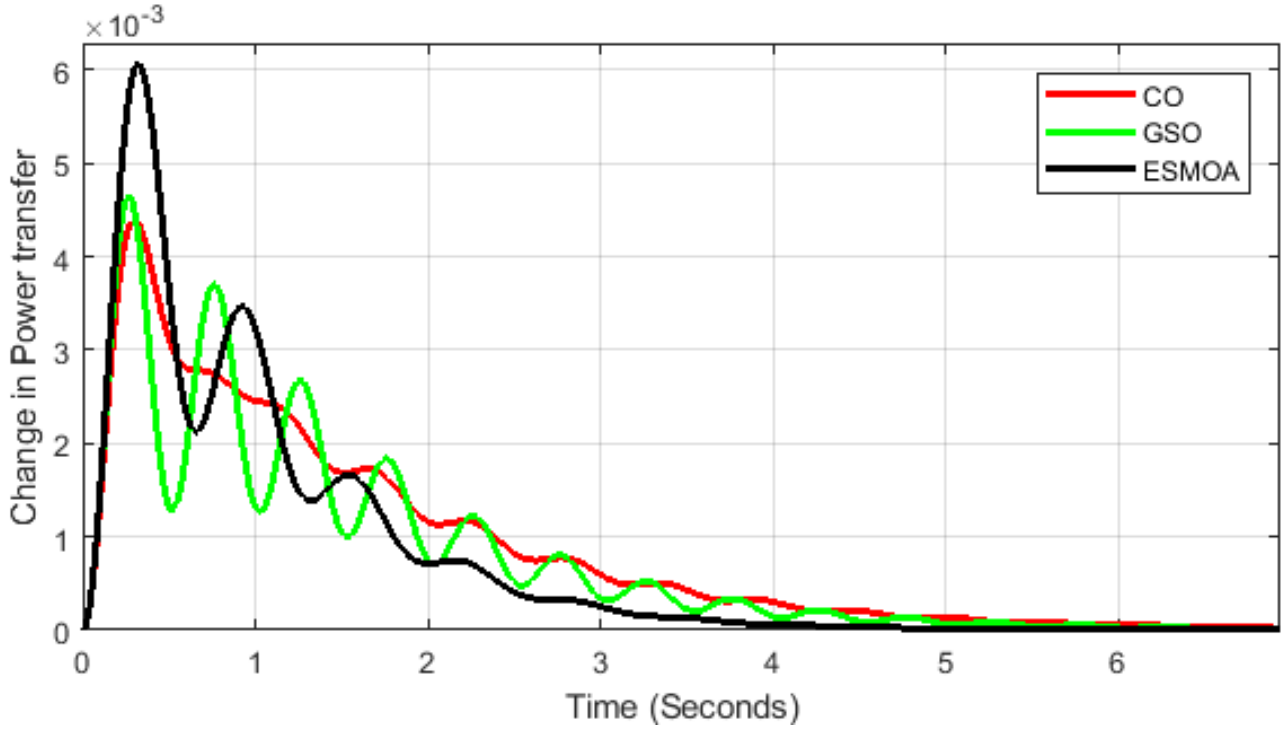

(**c**)

Figure 12. Dynamic responses for CO, GSO, and the proposed ESMOA for Case 3. (**a**) Deviation in frequency in area 1. (**b**) Deviation in frequency in area 2. (**c**) Deviation in transferred power through interconnected tie-line.

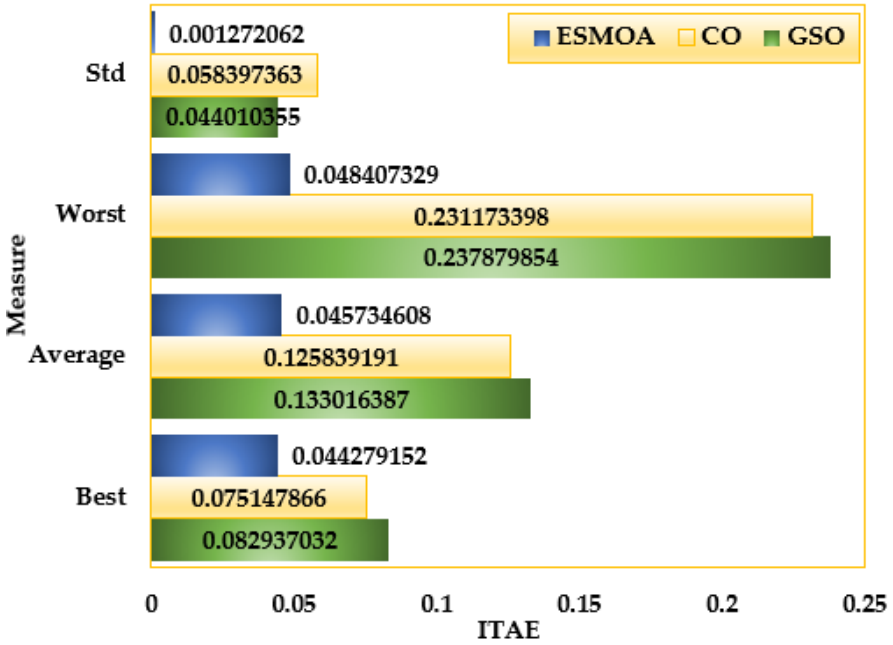

Figure 13. Statistical measures for CO, GSO, and the proposed ESMOA for Case 3.

Table 8 contrasts the efficacy of the proposed ESMOA-based PD-PI controller with various previously published controlling methods concerning ITAE. As shown, the proposed ESMOA-based PD-PI controller obtains the minimum ITAE of 0.04428, where the conventional PID-based-PSO, PID-based-ARA, PID-based-JAYA, PI-based-DE, PID-based-SAMPE-JAYA, CO-based PD-PI controller, and GSO-based PD-PI controller find 0.2354, 0.146308, 0.2272, 0.2021, 0.1726, 0.075148, and 0.082937, respectively.

Table 8. Comparison of the proposed ESMOA outcomes with other reported results in terms of ITAE for Case 3.

Controller	Optimization Technique	Reference	ITAE Objective Value
PID	PSO	[40]	0.2354
PID	ARA	[40]	0.146308
PID	JAYA	[40]	0.2272
PID	DE	[40]	0.2021
PID	SAMPE-JAYA	[40]	0.1726
PD-PI	CO	Applied	0.075148
PD-PI	GSO	Applied	0.082937
PD-PI	Proposed ESMOA	Applied	0.044279

Then, the proposed ESMOA results obtained using the cascaded PD-PI controller are compared with the other reported results that use different types of controllers, namely, PI and PID. The parameters of the compared controllers were optimized in previous articles based on other recent algorithms which simulated several operating scenarios of the same power system model. Therefore, all the controllers are adequately designed with the best parameters. This point demonstrates that the presented cascaded PD-PI controller, designed based on the proposed ESMOA, outperforms the same controller based on the GSO and CO. Additionally, the presented cascaded PD-PI controller, designed based on the proposed ESMOA, outperforms the PI and PID controllers, which were designed based on other previous algorithms.

4.2.4. Application for Case 4 as Extension to Non-Linear Power System

To further show the effectiveness of the proposed ESMOA in handling the frequency stability in power systems, the developed ESMOA is applied in comparison to GSO and CO for tuning the presented cascaded PD-PI controller considering the non-linearities in the power system model. This study was expanded to involve any non-linearity which could exist in the power grid. The non-linear characteristic is illustrated in Figure 14 as well as in [47]. Instead of the linear model of the non-reheat turbine displayed in Figure 1, the actual physical limit on the response speed of a turbine determined by the generation rate constraint (GRC) effect (δ) is integrated with 0.05 in this model. This is to account for the GRC impact (i.e., the practical physical constraint on the response speed of a turbine).

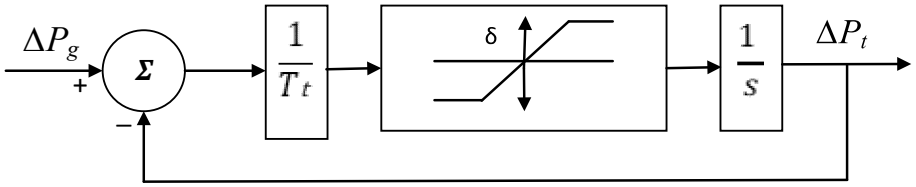

Figure 14. Non-linear turbine model with GRC.

At t = 0 s, a step load rise of 0.05 p.u. in area 1 is implemented for the above purpose. The proposed ESMOA, GSO, and CO methods are used, as shown in Figure 15, and Table 9 outlines the simulated data for the studied ITAE minimizing approaches. The summarized statistics are presented in addition to the ITAE goal scores and the associated parameter settings of K_{p1}, K_i, K_{p2}, K_d, and n in each area. According to the results, the suggested ESMOA has the lowest ITAE objective value of 0.225044, while CO and GSO have ITAE objective values of 0.230348 and 0.254536, respectively. As a result, the proposed ESMOA increases the ITAE value by 11.59% when compared to GSO and 2.31% when compared to CO.

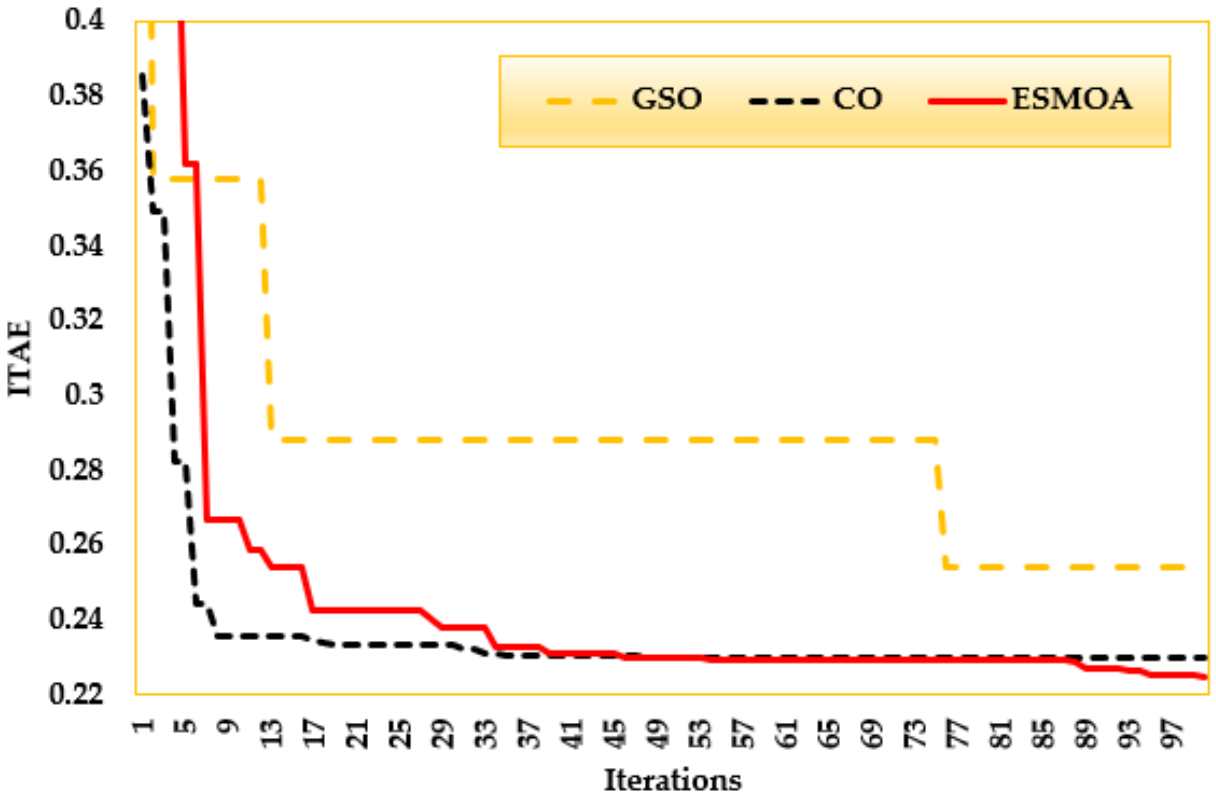

Figure 15. Convergence characteristics for CO, GSO, and the proposed ESMOA for Case 4.

Table 9. Results for Case 4.

Algorithm			Proposed ESMOA	GSO	CO
Controller parameters	K_{P1}	Area 1	1.810359	2.7	0.52778
	K_i		1.16859	1.8	0.988066
	K_{P2}		0.432614	0.3	1.44749
	K_d		1.078064	1.8	1.401102
	n		448.8788	201.3416	166.6564
	K_{P1}	Area 2	0.258859	0	2.5717
	K_i		1.875776	2.1	1.135735
	K_{P2}		0.516261	1.824008	1.692278
	K_d		1.50658	2.4	2.446288
	n		339.1538	301.3416	225.1243
ITAE Value			0.225044	0.254536	0.230348
ITAE improvement percent compared to the proposed ESMOA			-	11.59	2.31

For this case, Figure 16 depicts the assessed four measures of the lowest, mean, maximum, and standard deviation of the produced ITAE throughout several independent operations to provide statistical comparability between CO, GSO, and the suggested ESMOA. The suggested ESMOA is used to obtain the smallest measurements, as illustrated. It finds the smallest minimum, mean, maximum, and standard deviation with 0.225, 0.2314, 0.2375, and 0.0054, respectively.

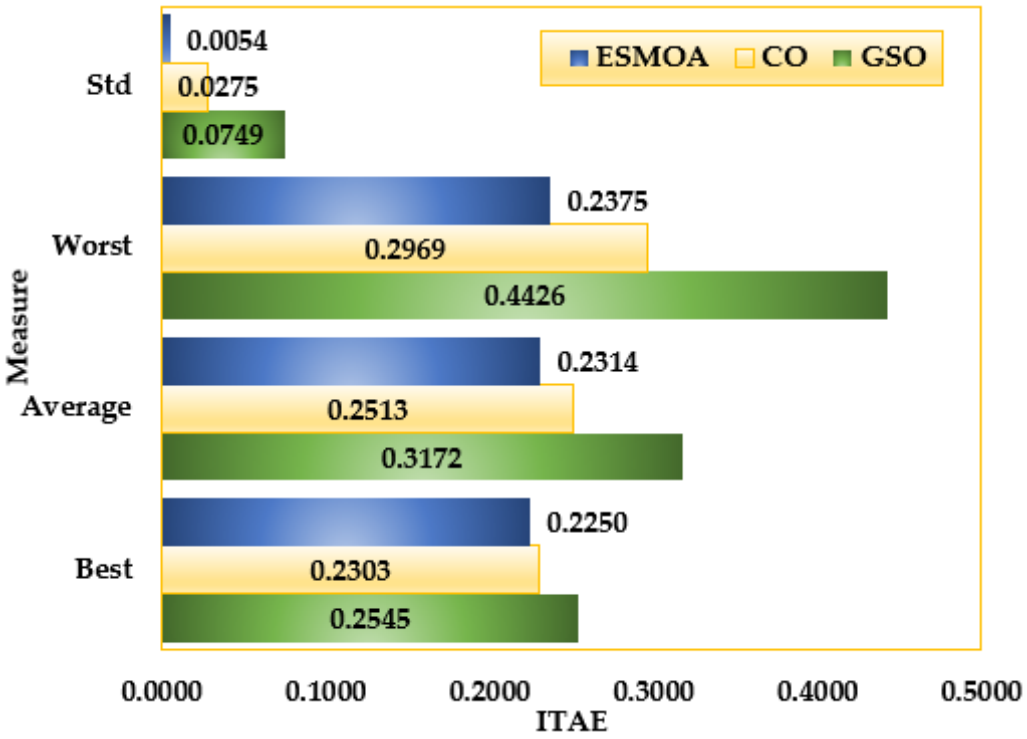

Figure 16. Statistical measures for CO, GSO, and the proposed ESMOA for Case 4.

Furthermore, the dynamic responses for frequency deviations in each area and tie-line power under ITAE are displayed in Figure 17. The proposed ESMOA provides better performances over CO and GSO in terms of settling times in frequency deviations and

tie-line power deviations. From Figure 17a, that displays the deviation in frequency in area 1, the proposed ESMOA shows a rise time of 1.8143×10^{-4} s; settling time of 2.8403 s; and peak time of 1.0750 s. From Figure 17b, that displays the deviation in frequency in area 2, the proposed ESMOA records the minimum settling time of 2.7745 s, while the CO and GSO record settling times of 2.9972 and 3.3071 s. Additionally, the proposed ESMOA achieves the least peak time of 1.0232 s as shown in Figure 17c, that displays the deviation in power transfer between the two areas, while the CO and GSO record peak times of 1.0482 and 0.0383 s.

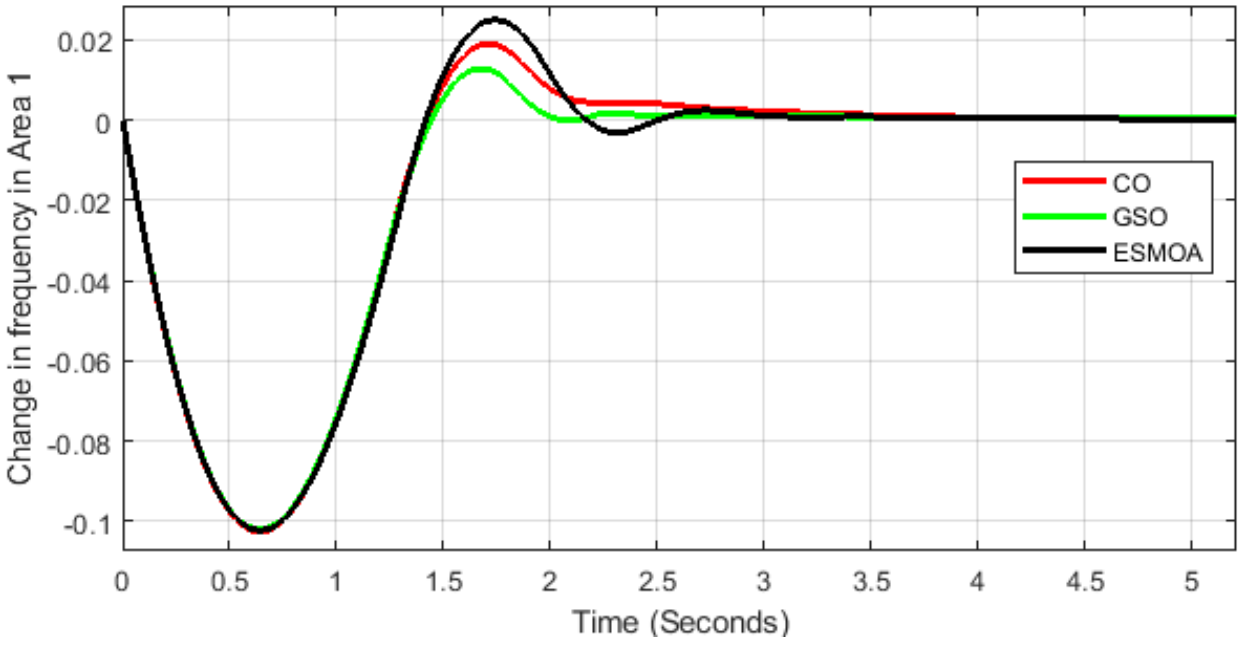

(**a**)

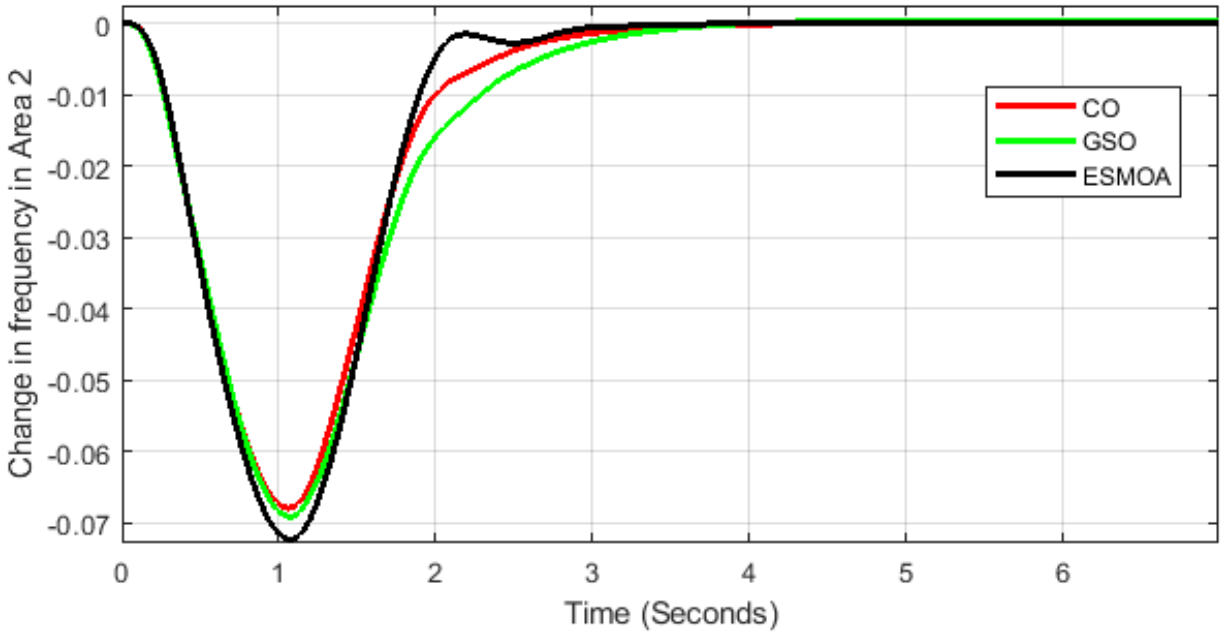

(**b**)

Figure 17. *Cont.*

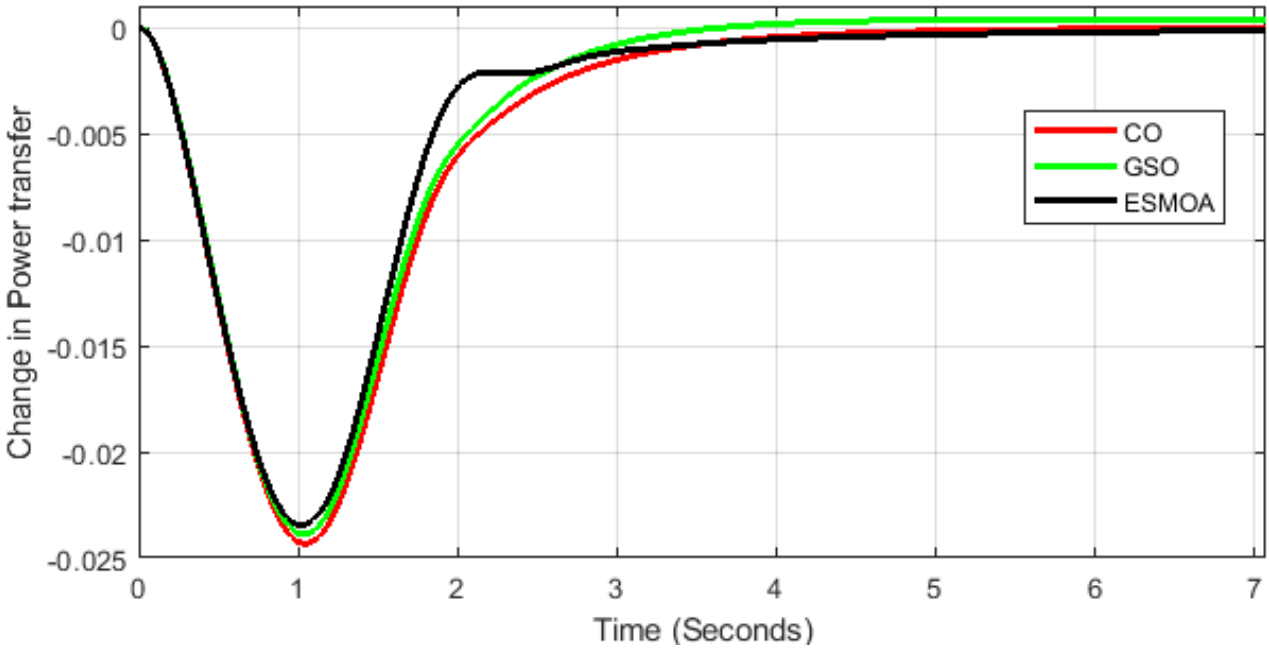

(**c**)

Figure 17. Dynamic responses for CO, GSO, and the proposed ESMOA for Case 4. (**a**) Deviation in frequency in area 1. (**b**) Deviation in frequency in area 2. (**c**) Deviation in transferred power through interconnected tie-line.

Table 10 contrasts the efficacy of the proposed ESMOA-based PD-PI controller with various previously published controlling methods concerning ITAE. As shown, the proposed ESMOA-based PD-PI controller obtains the minimum ITAE of 0.225044, while the conventional PID, PID-based-GA, PID-based-BFOA, PID-based-FA, PID-based-hybrid FA and pattern search, CO-based PD-PI controller, and GSO-based PD-PI controller find 0.604, 0.5513, 0.4788, 0.324, 0.2782, 0.230348, and 0.25436, respectively.

Table 10. Comparison of the proposed ESMOA outcomes with other reported results in terms of ITAE for Case 4.

Controller	Optimization Technique	Reference	ITAE Objective Value
PID	Conventional	[47]	0.604
PID	GA	[47]	0.5513
PID	BFOA	[47]	0.4788
PID	FA	[48]	0.324
PID	hybrid FA and pattern search	[48]	0.2782
PD-PI	CO	Applied	0.230348
PD-PI	GSO	Applied	0.25436
PD-PI	Proposed ESMOA	Applied	0.225044

5. Conclusions

This paper presents a cascaded PD-PI controller optimized using an improved ESMOA, which includes a chaotic dynamic and an elite group. The suggested cascaded PD-PI controller based on the ESMOA solves the FSP in MAPSs with two area non-reheat thermal systems. The motion update incorporates the chaotic technique, and the exploitation procedure is enhanced by searching for an elite group rather than merely the best solution overall.

The proposed ESMOA is assessed compared to GSO and CO for designing the cascaded PD-PI controller. The proposed ESMOA provides the best performance. For load perturbation in area 1, the proposed ESMOA improves the ITAE value by 12.48% and 2.0521% compared to GSO and CO, respectively. For load perturbation in area 2, the proposed ESMOA enhances the ITAE value by 10% and 0.71% compared to GSO and CO, respectively. For simultaneous load perturbation in areas 1 and 2, the suggested ESMOA improves the ITAE value by 41.1% and 46.61% compared to GSO and CO, respectively. Additionally, the proposed ESMOA shows higher robustness than CO and GSO as it successfully finds the smallest minimum, mean, maximum, and standard deviation. In addition to that, the effectiveness of the presented cascaded PD-PI controller via the proposed ESMOA is demonstrated in handling the frequency stability considering the non-linearities in the power system model. Moreover, the proposed cascaded PD-PI controller based on the ESMOA demonstrates significant efficiency and outperformance over several previously published PID and PI controllers adjusted using numerous contemporary techniques.

Author Contributions: Conceptualization, A.R.G.; Methodology, S.A., M.E. and A.R.G.; Software, A.R.G.; Validation, A.M.E.-R., A.M.S., G.M. and M.A.T.; Formal analysis, S.A., A.M.E.-R., G.M. and M.A.T.; Investigation, A.M.E.-R., M.E., G.M. and M.A.T.; Resources, M.E.; Data curation, A.M.S. and M.A.T.; Writing—original draft, S.A.; Writing—review & editing, A.M.E.-R. and M.E.; Visualization, A.M.S. All authors have read and agreed to the published version of the manuscript.

Funding: This research received no external funding.

Data Availability Statement: Not applicable.

Conflicts of Interest: The authors declare no conflict of interest.

References

1. Mehta, S.; Basak, P. A comprehensive review on control techniques for stability improvement in microgrids. *Int. Trans. Electr. Energy Syst.* **2021**, *31*, e12822. [CrossRef]
2. Sharma, D. Load Frequency Control: A Literature Review. *Int. J. Sci. Technol. Res.* **2020**, *9*, 6421–6437.
3. Hassan, A.; Aly, M.; Elmelegi, A.; Nasrat, L.; Watanabe, M.; Mohamed, E.A. Optimal Frequency Control of Multi-Area Hybrid Power System Using New Cascaded TID-PI$^{\lambda}$D$^{\mu}$N Controller Incorporating Electric Vehicles. *Fractal Fract.* **2022**, *6*, 548. [CrossRef]
4. Elkasem, A.H.A.; Khamies, M.; Hassan, M.H.; Agwa, A.M.; Kamel, S. Optimal Design of TD-TI Controller for LFC Considering Renewables Penetration by an Improved Chaos Game Optimizer. *Fractal Fract.* **2022**, *6*, 220. [CrossRef]
5. Nayak, J.R.; Shaw, B.; Sahu, B.K. Implementation of hybrid SSA–SA based three-degree-of-freedom fractional-order PID controller for AGC of a two-area power system integrated with small hydro plants. *IET Gener. Transm. Distrib.* **2020**, *14*, 2430–2440. [CrossRef]
6. Naidu, K.; Mokhlis, H.; Abu Bakar, A.H.; Terzija, V. Performance investigation of ABC algorithm in multi-area power system with multiple interconnected generators. *Appl. Soft Comput.* **2017**, *57*, 436–451. [CrossRef]
7. El-Ela, A.A.A.; El-Sehiemy, R.A.; Shaheen, A.M.; Ellien, A.R. Review on Active Distribution Networks with Fault Current Limiters and Renewable Energy Resources. *Energies* **2022**, *15*, 7648. [CrossRef]
8. Ginidi, A.; Elattar, E.; Shaheen, A.; Elsayed, A.; El-Sehiemy, R.; Dorrah, H. Optimal Power Flow Incorporating Thyristor-Controlled Series Capacitors Using the Gorilla Troops Algorithm. *Int. Trans. Electr. Energy Syst.* **2022**, *2022*, 9448199. [CrossRef]
9. Mohammadi, F.; Nazri, G.-A.; Saif, M. An Improved Mixed AC/DC Power Flow Algorithm in Hybrid AC/DC Grids with MT-HVDC Systems. *Appl. Sci.* **2020**, *10*, 297. [CrossRef]
10. El-Sehiemy, R.; Hamida, M.A.; Elattar, E.; Shaheen, A.; Ginidi, A. Nonlinear Dynamic Model for Parameter Estimation of Li-Ion Batteries Using Supply–Demand Algorithm. *Energies* **2022**, *15*, 4556. [CrossRef]
11. Nasef, A.; Shaheen, A.; Khattab, H. Local and remote control of automatic voltage regulators in distribution networks with different variations and uncertainties: Practical cases study. *Electr. Power Syst. Res.* **2022**, *205*, 107773. [CrossRef]
12. Bevrani, H.; Golpîra, H.; Messina, A.R.; Hatziargyriou, N.; Milano, F.; Ise, T. Power system frequency control: An updated review of current solutions and new challenges. *Electr. Power Syst. Res.* **2021**, *194*, 107114. [CrossRef]
13. Mohamed, T.H.; Alamin, M.A.M.; Hassan, A.M. A novel adaptive load frequency control in single and interconnected power systems. *Ain Shams Eng. J.* **2020**, *12*, 1763–1773. [CrossRef]
14. Naidu, K.; Mokhlis, H.; Bakar, A. Multiobjective optimization using weighted sum Artificial Bee Colony algorithm for Load Frequency Control. *Int. J. Electr. Power Energy Syst.* **2014**, *55*, 657–667. [CrossRef]
15. Hasan, N.; Nasirudin, I.; Farooq, S. Hybrid Taguchi Genetic Algorithm-Based AGC Controller for Multisource Interconnected Power System. *Electr. Power Compon. Syst.* **2019**, *47*, 101–112. [CrossRef]

16. Bhatt, P.; Roy, R.; Ghoshal, S. GA/particle swarm intelligence based optimization of two specific varieties of controller devices applied to two-area multi-units automatic generation control. *Int. J. Electr. Power Energy Syst.* **2010**, *32*, 299–310. [CrossRef]
17. Rout, U.K.; Sahu, R.K.; Panda, S. Design and analysis of differential evolution algorithm based automatic generation control for interconnected power system. *Ain Shams Eng. J.* **2013**, *4*, 409–421. [CrossRef]
18. Jagatheesan, K.; Anand, B.; Samanta, S.; Dey, N.; Santhi, V.; Ashour, A.S.; Balas, V.E. Application of flower pollination algorithm in load frequency control of multi-area interconnected power system with nonlinearity. *Neural Comput. Appl.* **2017**, *28*, 475–488. [CrossRef]
19. Panda, S.; Mohanty, B.; Hota, P. Hybrid BFOA–PSO algorithm for automatic generation control of linear and nonlinear interconnected power systems. *Appl. Soft Comput.* **2013**, *13*, 4718–4730. [CrossRef]
20. Guo, J. Application of a novel adaptive sliding mode control method to the load frequency control. *Eur. J. Control* **2020**, *57*, 172–178. [CrossRef]
21. Sharma, Y.; Saikia, L.C. Automatic generation control of a multi-area ST—Thermal power system using Grey Wolf Optimizer algorithm based classical controllers. *Int. J. Electr. Power Energy Syst.* **2015**, *73*, 853–862. [CrossRef]
22. Abdelaziz, A.; Ali, E. Cuckoo Search algorithm based load frequency controller design for nonlinear interconnected power system. *Int. J. Electr. Power Energy Syst.* **2015**, *73*, 632–643. [CrossRef]
23. Dash, P.; Saikia, L.C.; Sinha, N. Comparison of performances of several Cuckoo search algorithm based 2DOF controllers in AGC of multi-area thermal system. *Int. J. Electr. Power Energy Syst.* **2014**, *55*, 429–436. [CrossRef]
24. El Ela, A.A.A.; El-Sehiemy, R.A.; Shaheen, A.M.; Diab, A.E.G. Optimal Design of PID Controller Based Sampe-Jaya Algorithm for Load Frequency Control of Linear and Nonlinear Multi-Area Thermal Power Systems. *Int. J. Eng. Res. Afr.* **2020**, *50*, 79–93. [CrossRef]
25. Singh, S.P.; Prakash, T.; Singh, V.; Babu, M.G. Analytic hierarchy process based automatic generation control of multi-area interconnected power system using Jaya algorithm. *Eng. Appl. Artif. Intell.* **2017**, *60*, 35–44. [CrossRef]
26. Pati, T.K.; Nayak, J.R.; Sahu, B.K. Application of TLBO algorithm to study the performance of automatic generation control of a two-area multi-units interconnected power system. In Proceedings of the 2015 IEEE International Conference on Signal Processing, Informatics, Communication and Energy Systems, SPICES, Kozhikode, India, 19–21 February 2015; pp. 1–5. [CrossRef]
27. Li, S.; Chen, H.; Wang, M.; Heidari, A.A.; Mirjalili, S. Slime mould algorithm: A new method for stochastic optimization. *Future Gener. Comput. Syst.* **2020**, *111*, 300–323. [CrossRef]
28. El-Ela, A.A.A.; El-Sehiemy, R.A.; Shaheen, A.M.; Diab, A.E.-G. Enhanced coyote optimizer-based cascaded load frequency controllers in multi-area power systems with renewable. *Neural Comput. Appl.* **2021**, *33*, 8459–8477. [CrossRef]
29. Zheng, J.; Xie, Y.; Huang, X.; Wei, Z.; Taheri, B. Balanced version of Slime Mold Algorithm: A study on PEM fuel cell system parameters identification. *Energy Rep.* **2021**, *7*, 3199–3209. [CrossRef]
30. Yu, K.; Liu, L.; Chen, Z. An Improved Slime Mould Algorithm for Demand Estimation of Urban Water Resources. *Mathematics* **2021**, *9*, 1316. [CrossRef]
31. Dhawale, D.; Kamboj, V.K.; Anand, P. An effective solution to numerical and multi-disciplinary design optimization problems using chaotic slime mold algorithm. *Eng. Comput.* **2021**, *38*, 2739–2777. [CrossRef]
32. Mostafa, M.; Rezk, H.; Aly, M.; Ahmed, E.M. A new strategy based on slime mould algorithm to extract the optimal model parameters of solar PV panel. *Sustain. Energy Technol. Assess.* **2020**, *42*, 100849. [CrossRef]
33. Liu, Y.; Heidari, A.A.; Ye, X.; Liang, G.; Chen, H.; He, C. Boosting slime mould algorithm for parameter identification of photovoltaic models. *Energy* **2021**, *234*, 121164. [CrossRef]
34. Sarhan, S.; Shaheen, A.M.; El-Sehiemy, R.A.; Gafar, M. An Enhanced Slime Mould Optimizer That Uses Chaotic Behavior and an Elitist Group for Solving Engineering Problems. *Mathematics* **2022**, *10*, 1991. [CrossRef]
35. Khunkitti, S.; Siritaratiwat, A.; Premrudeepreechacharn, S. Multi-Objective Optimal Power Flow Problems Based on Slime Mould Algorithm. *Sustainability* **2021**, *13*, 7448. [CrossRef]
36. Hassan, M.H.; Kamel, S.; Abualigah, L.; Eid, A. Development and application of slime mould algorithm for optimal economic emission dispatch. *Expert Syst. Appl.* **2021**, *182*, 115205. [CrossRef]
37. Noroozi, M.; Mohammadi, H.; Efatinasab, E.; Lashgari, A.; Eslami, M.; Khan, B. Golden Search Optimization Algorithm. *IEEE Access* **2022**, *10*, 37515–37532. [CrossRef]
38. Qais, M.H.; Hasanien, H.M.; Turky, R.A.; Alghuwainem, S.; Tostado-Véliz, M.; Jurado, F. Circle Search Algorithm: A Geometry-Based Metaheuristic Optimization Algorithm. *Mathematics* **2022**, *10*, 1626. [CrossRef]
39. Xu, Y.; Li, C.; Wang, Z.; Zhang, N.; Peng, B. Load Frequency Control of a Novel Renewable Energy Integrated Micro-Grid Containing Pumped Hydropower Energy Storage. *IEEE Access* **2018**, *6*, 29067–29077. [CrossRef]
40. El-Sehiemy, R.; Shaheen, A.; Ginidi, A.; Al-Gahtani, S.F. Proportional-Integral-Derivative Controller Based-Artificial Rabbits Algorithm for Load Frequency Control in Multi-Area Power Systems. *Fractal Fract.* **2023**, *7*, 97. [CrossRef]
41. Dash, P.; Saikia, L.C.; Sinha, N. Flower Pollination Algorithm Optimized PI-PD Cascade Controller in Automatic Generation Control of a Multi-area Power System. *Int. J. Electr. Power Energy Syst.* **2016**, *82*, 19–28. [CrossRef]
42. El-Ela, A.A.A.; El-Sehiemy, R.A.; Shaheen, A.M.; Diab, A.E.-G. Design of cascaded controller based on coyote optimizer for load frequency control in multi-area power systems with renewable sources. *Control Eng. Pract.* **2022**, *121*, 105058. [CrossRef]

43. Alhelou, H.H.; Hamedani-Golshan, M.E.; Heydarian-Forushani, E.; Al-Sumaiti, A.S.; Siano, P. Decentralized Fractional Order Control Scheme for LFC of Deregulated Nonlinear Power Systems in Presence of EVs and RER. In Proceedings of the 2018 International Conference on Smart Energy Systems and Technologies, SEST 2018 Proceedings, Sevilla, Spain, 10–12 September 2018; pp. 1–6. [CrossRef]
44. Kumari, S.; Chugh, R. A novel four-step feedback procedure for rapid control of chaotic behavior of the logistic map and unstable traffic on the road. *Chaos* **2020**, *30*, 123115. [CrossRef] [PubMed]
45. Wu, G.; Mallipeddi, R.; Suganthan, P.N. *Problem Definitions and Evaluation Criteria for the CEC 2017 Competition on Constrained Real Parameter Optimization*; Technical Report; National University of Defense Technology: Changsha, China; Kyungpook National University: Daegu, Republic of Korea; Nanyang Technological University: Singapore, 2017.
46. Padhan, S.; Sahu, R.K.; Panda, S. Application of Firefly Algorithm for Load Frequency Control of Multi-Area Interconnected Power System. *Electr. Power Compon. Syst.* **2014**, *42*, 1419–1430. [CrossRef]
47. Ali, E.; Abd-Elazim, S. BFOA based design of PID controller for two area Load Frequency Control with nonlinearities. *Int. J. Electr. Power Energy Syst.* **2013**, *51*, 224–231. [CrossRef]
48. Sahu, R.K.; Panda, S.; Padhan, S. A hybrid firefly algorithm and pattern search technique for automatic generation control of multi area power systems. *Int. J. Electr. Power Energy Syst.* **2015**, *64*, 9–23. [CrossRef]